

Air Force Institute of Technology

**AFIT Scholar**

---

Theses and Dissertations

Student Graduate Works

---

3-2006

## Non-Cooperative Detection of Frequency-Hopped GMSK Signals

Clint R. Sikes

Follow this and additional works at: <https://scholar.afit.edu/etd>



Part of the [Signal Processing Commons](#)

---

### Recommended Citation

Sikes, Clint R., "Non-Cooperative Detection of Frequency-Hopped GMSK Signals" (2006). *Theses and Dissertations*. 3506.

<https://scholar.afit.edu/etd/3506>

This Thesis is brought to you for free and open access by the Student Graduate Works at AFIT Scholar. It has been accepted for inclusion in Theses and Dissertations by an authorized administrator of AFIT Scholar. For more information, please contact [richard.mansfield@afit.edu](mailto:richard.mansfield@afit.edu).



**NON-COOPERATIVE DETECTION OF  
FREQUENCY-HOPPED GMSK SIGNALS**

THESIS

Clint R. Sikes, First Lieutenant, USAF

AFIT/GE/ENG/06-52

**DEPARTMENT OF THE AIR FORCE  
AIR UNIVERSITY**

***AIR FORCE INSTITUTE OF TECHNOLOGY***

**Wright-Patterson Air Force Base, Ohio**

APPROVED FOR PUBLIC RELEASE; DISTRIBUTION UNLIMITED

The views expressed in this thesis are those of the author and do not reflect the official policy or position of the United States Air Force, Department of Defense, or the United States Government.

AFIT/GE/ENG/06-52

NON-COOPERATIVE DETECTION OF FREQUENCY-HOPPED GMSK SIGNALS

THESIS

Presented to the Faculty

Department of Electrical and Computer Engineering

Graduate School of Engineering and Management

Air Force Institute of Technology

Air University

Air Education and Training Command

In Partial Fulfillment of the Requirements for the  
Degree of Master of Science in Electrical Engineering

Clint R. Sikes, BSEE

First Lieutenant, USAF

March 2006

APPROVED FOR PUBLIC RELEASE; DISTRIBUTION UNLIMITED.


NON-COOPERATIVE DETECTION OF GMSK FREQUENCY-HOPPED SIGNALS

Clint R. Sikes, BSEE  
First Lieutenant, USAF

Approved:

  
\_\_\_\_\_  
Robert F. Mills, Ph.D. (Chairman)

6 MAR 06  
Date

  
\_\_\_\_\_  
Michael A. Temple, Ph.D. (Member)

3 Mar 06  
Date

  
\_\_\_\_\_  
Stewart L. DeVilbiss, Lt Col, USAF (Member)

3 Mar 06  
Date

## Table of Contents

	Page
List of Figures .....	vii
List of Tables .....	ix
Abstract .....	x
1. Introduction .....	1-1
1.1 Introduction .....	1-1
1.2 Problem Statement .....	1-1
1.3 Research Assumptions .....	1-2
1.4 Research Scope .....	1-3
1.5 Research Approach .....	1-3
1.6 Materials and Equipment .....	1-5
1.7 Thesis Organization .....	1-5
2. Background .....	2-1
2.1 Introduction .....	2-1
2.2 Tactical Communication Scenario .....	2-1
2.3 Communication Link .....	2-2
2.3.1 Frequency Hopping (FH) .....	2-4

	Page
2.3.2 Gaussian Minimum Shift Keying (GMSK).....	2-6
2.3.2.1 MSK.....	2-6
2.3.2.2 GMSK Defined.....	2-6
2.4 Interception Link.....	2-9
2.4.1 Non-Cooperative Detection Overview .....	2-11
2.4.2 Wideband Radiometer .....	2-12
2.4.3 Channelized Radiometer.....	2-15
2.5 Quality Factors.....	2-19
2.6 Summary.....	2-20
3. Methodology .....	3-1
3.1 Introduction.....	3-1
3.2 Signal Structure.....	3-1
3.2.1 Signal Generation .....	3-1
3.2.2 Signal Parameters .....	3-2
3.2.3 Intentional Jitter.....	3-3
3.3 Intercept Receiver Processing.....	3-3
3.3.1 Wideband Radiometer .....	3-4
3.3.2 Channelized Radiometer.....	3-6
3.3.2.1 Narrow Bandwidth Channelized Radiometer .....	3-9
3.3.2.2 Sweeping Channelized Radiometer.....	3-9

	Page
3.4 Delay and Multiply Receiver .....	3-12
3.5 Jamming Transmitters.....	3-13
3.5.1 Wideband Jammer .....	3-13
3.5.2 Narrowband Jammer .....	3-14
3.6 Summary .....	3-14
4. Detection Results and Analysis .....	4-1
4.1 Introduction.....	4-1
4.2 Wideband Baseline for Comparison .....	4-1
4.3 Effects of Changing Signal Parameters on Detection Performance .....	4-3
4.3.1 Altering Signal Duration.....	4-3
4.3.2 Altering Hop Rate .....	4-5
4.3.3 Altering Jitter .....	4-7
4.4 Changes to the Standard Channelized Radiometer Model .....	4-9
4.4.1 Narrow-Bandwidth Channelized Radiometer.....	4-9
4.4.2 Sweeping Channelized Radiometer .....	4-11
4.5 Jamming.....	4-13
4.5.1 Wideband Jamming .....	4-13
4.5.2 Narrowband Jamming.....	4-16
4.6 Summary .....	4-19



	Page
5. Conclusions .....	5-1
5.1 Summary .....	5-1
5.2 Conclusions.....	5-2
5.2.1 Scenarios Beneficial to the Communicating Party .....	5-2
5.2.2 Scenarios Beneficial to the Intercepting Party.....	5-3
5.3 Recommendations for Future Research.....	5-3
5.3.1 Introduce Doppler Shifting .....	5-3
5.3.2 Recognize Multiple Signals in the Environment.....	5-4
5.3.3 Use Actual Signal Data.....	5-4
5.3.4 Use Multiple Antennas .....	5-5
 Appendix A. Delay and Multiply Receiver Results .....	 A-1
A.1 Baseline Signal Parameters.....	A-1
A.2 Reducing Signal Duration.....	A-2
A.3 Reducing Hop Rate .....	A-3
A.4 Introducing Wideband Jamming.....	A-3
 Appendix B. MATLAB Code .....	 B-1
 Bibliography .....	 BIB-1

## List of Figures

Figure	Page
2.1 Tactical Communication Scenario .....	2-1
2.2 Representative Bit Error Curve Plot .....	2-4
2.3 FH Signal Space.....	2-5
2.4 GMSK Pulses.....	2-7
2.5 Plot of GMSK Signal .....	2-8
2.6 Input Data vs. Phase, GMSK Modulation .....	2-9
2.7 Simulated PSDs of BPSK and GMSK.....	2-9
2.8 Wideband Radiometer Block Diagram.....	2-12
2.9 Chi-Square PDFs of Noise and Signal Plus Noise .....	2-13
2.10 Channelized Radiometer Block Diagram (Binary-OR).....	2-16
3.1 GMSK Generation Block Diagram.....	3-1
3.2 Simulated Wideband Radiometer Block Diagram.....	3-4
3.3 Sample Statistics Used for Thresholding.....	3-4
3.4 Wideband Radiometer, Theoretical vs. Simulated .....	3-5
3.5 Simulated Channelized Block Diagram.....	3-7
3.6 Channelized Radiometer: Theoretical vs. Simulated.....	3-8
3.7 Sweeping Channelized Radiometer .....	3-10
3.8 Simulated Fast Sweeping Channelized Radiometer Block Diagram.....	3-11
3.9 Delay and Multiply Receiver Block Diagram .....	3-12
3.10 Chip Rate Detector Feature Generation.....	3-13

Figure	Page
4.1 Wideband Radiometer, $T_I=96$ bits, $W_I=30$ Hz, and $P_{FA}=0.01$ .....	4-2
4.2 Wideband vs Channelized Radiometer, $T_I=96$ bits .....	4-3
4.3 Wideband vs. Channelized Radiometer, $T_I=40$ .....	4-4
4.4 Varying $T_I$ form 30 bits to 100 bits .....	4-5
4.5 Wideband vs. Channelized Radiometer, $T_2=32$ bits .....	4-6
4.6 Varying Hop Rate (1/20 hops/sec to 1 hop/sec) .....	4-7
4.7 Channelized vs. Wideband Radiometer, Jitter=25% .....	4-8
4.8 Varying Jitter 5% to 50 %.....	4-9
4.9 Channelized vs. Wideband, Narrow BW .....	4-10
4.10 Wideband Radiometer vs. Slow-Sweep Channelized Radiometer .....	4-12
4.11 Wideband vs. Both Sweeping Channelized Radiometers.....	4-13
4.12 Wideband Radiometer with Wideband Jamming .....	4-15
4.13 Channelized Radiometer with Wideband Jamming.....	4-15
4.14 Wideband vs. Channelized Radiometer with Wideband Jamming.....	4-16
4.15 Wideband Radiometer with Narrowband Jamming.....	4-17
4.16 Channelized Radiometer with Narrowband Jamming .....	4-18
4.17 Wideband vs. Channelized Radiometer with Narrowband Jamming .....	4-18
A.1 Baseline D&M .....	A-1
A.2 D&M Reduction in $T_I$ from 96 to 40 Bits.....	A-2
A.3 D&M Reduction in Hop Rate from 1/8 to 1/32 Seconds.....	A-3
A.4 D&M With Wideband Jamming .....	A-3

## List of Tables

Table	Page
4.1 Summary of Test Results .....	4-19
5.1 Tested Parameters .....	5-1

### Abstract

Many current and emerging communication signals use Gaussian Minimum Shift Keyed (GMSK), Frequency-Hopped (FH) waveforms to reduce adjacent-channel interference while maintaining Low Probability of Intercept (LPI) characteristics. These waveforms appear in both military (Tactical Targeting Networking Technology, or TTNT) and civilian (Bluetooth) applications. This research develops wideband and channelized radiometer intercept receiver models to detect a GMSK-FH signal under a variety of conditions in a tactical communications environment. The signal of interest (SOI) and receivers have both fixed and variable parameters. Jamming is also introduced into the system to serve as an environmental parameter. These parameters are adjusted to examine the effects they have on the detectability of the SOI. The metric for detection performance is the distance the intercept receiver must be from the communication transmitter in order to meet a given set of intercept receiver performance criteria, e.g.,  $P_{FA}$  and  $P_D$ . It is shown that the GMSK-FH waveform benefits from an increased hop rate, a reduced signal duration, and introducing jitter into the waveform. Narrowband jamming is also very detrimental to channelized receiver performance. The intercept receiver benefits from reducing the bandwidth of the channelized radiometer channels, although this requires precise *a priori* knowledge of the hop frequencies.

## **1. Introduction**

### **1.1 Introduction**

Since October 1994 the United States Department of Defense (DoD) has been using the Link 16 tactical data link for its major Command, Control, and Intelligence (C2I) systems. The number of platforms expected to use the Link-16 system for transmitting and receiving secure voice and data is continually rising and is expected to do so until FY2015 [1]. However, interoperability issues with civilian aviation data links (CADLs) and bandwidth limitations has encouraged the DoD to pursue alternative systems, most notably the Joint Tactical Radio System (JTRS).

A key feature of JTRS is its ability to merge legacy military data links, CADLs, and emerging military links into one system. One such emerging military data link is Tactical Targeting Network Technology, which merges the information flow between sensors and aircraft platforms [2]. The TTNT waveform should be a Low Probability of Intercept (LPI) waveform due to the sensitive nature of the material it carries. Thus, it would be highly beneficial to study the detectability characteristics of the TTNT waveform.

### **1.2 Problem Statement**

The TTNT signal uses a Frequency-Hopped Gaussian Minimum Shift Keying (GMSK) modulated waveform with both variable and fixed parameters. The waveform parameters should be adjusted such that it will be difficult to be detected by intercept receivers while also being resistant to jamming. Similarly, since many modern

communication systems are using GMSK modulation (i.e., Bluetooth and GSM), it would be beneficial for an intercept receiver to adjust its parameters to be able to detect and possibly exploit such signals. This research focuses on non-cooperative detection techniques for FH-GMSK signals.

### **1.3 Research Assumptions**

The following assumptions were made throughout this research:

- The channel is being modeled as stationary additive white Gaussian Noise (AWGN).
- Only one communication signal was present at a time. When jamming was introduced, only one jamming signal was present at a time (in conjunction with the communication signal). By using only one signal at a time, the environment becomes simple to model. Multiple signals are likely to interfere with each other and cause complications for all parties.
- All signals (communication and jamming) were modeled as line-of-sight transmissions with no multipath, which simplifies the problem of having multiple delayed and attenuated versions of a signal arriving at the receivers.
- The communication signal undergoes no change in performance (i.e., probability of bit error) with changes in signal parameters. In an actual communication system, changes in the signal environment will lead to changes in processing techniques if the performance is to remain the same.
- All bandpass channel filtering used ideal square filters and were centered at the hop frequencies of the transmitted communication signal. Real filters using

windowing techniques will degrade the receiver's performance slightly, but not enough to warrant detailed investigation in this research.

- In the cases where constant false alarm rate (CFAR) processing was used, the probability of false alarm ( $P_{FA}$ ) was maintained at a constant of 0.01.

#### **1.4 Research Scope**

Common intercept receiver architectures were developed for the purpose of detecting the GMSK-FH signal of interest (SOI) under a variety of conditions. A baseline scenario was established as a basis of comparison. Three types of variables were examined: signal parameters, receiver parameters, and the presence of jamming. The variables were tested for the different intercept receivers independently of one another to examine the relative effects of each variable on the detectability of the SOI. The results were compared to determine the set of parameters that were most beneficial to the communicating party and the set of parameters that were most beneficial to the intercepting party.

#### **1.5 Research Approach**

A typical tactical communication scenario is presented that includes a communication receiver, a communication transmitter, an intercept receiver, and jamming transmitters. The communication and interception links are examined separately, with equations governing the relative performance of each presented. The two links are combined to determine various LPI quality factors that relate the signal to noise ratio (SNR) of the environment to the distance from the communication transmitter at which the intercept receiver can achieve a set of performance criteria with the performance criteria of the communication link remaining a fixed quantity.



Two intercept receiver models (the wideband radiometer and the channelized radiometer) are then developed using both theoretical equations and computer simulations to detect the SOI. The wideband radiometer assumes *a priori* knowledge of the signal's overall signal duration and bandwidth, whereas the channelized radiometer has additional *a priori* knowledge of the signal's hop positions and channel locations. The SOI undergoes a series of alterations based on the variability of the TTNT waveform: signal duration, hop rate, and intentional jitter. Each alteration is tested on both receiver models. The same procedure is followed using receiver parameters such as narrowing the bandwidth of the channels in the channelized radiometer and reducing the number of channels available to the channelized radiometer. Finally, wideband and narrowband jamming transmitters are introduced into the system.

The results for the above tests are then compared to a baseline signal/receiver set to examine the relativistic detectability changes that occur. For each case, both the general detectability of the signal and the relative performance of the two receiver models are examined. The communicating party's goal is to adjust the environment such that the intercept receivers are forced to move in closer to the communication transmitter to achieve desired performance goals (thereby giving the interceptors a greater physical exposure to the communicating party's defenses). The intercepting party's goals are to be able to move away from the communication transmitter to achieve the given criteria and to achieve higher performance with the channelized radiometer versus the wideband radiometer as it is more sophisticated and has greater potential to exploit the signal.

## **1.6 Materials and Equipment**

All signals and receiver architectures presented in this research were simulated using MATLAB<sup>®</sup> Version 7.0 developed by Mathworks, Inc. The simulations were performed on a 3.0 GHz Pentium 4 PC.

## **1.7 Thesis Organization**

Chapter 2 provides background information on the communication and interception links encountered in a typical tactical communication scenario. The communication and interception range equations are also developed, culminating in LPI quality factors that were used to determine the effectiveness of each change in signal, intercept receiver, and jamming parameters. The development of the GMSK modulation scheme was presented to include advantages over classic phase shift keying techniques. Frequency-hopping was introduced to illustrate the LPI technique used for this particular signal of interest. Finally, theoretical models for both the wideband and channelized radiometers were developed. Chapter 3 discusses the GMSK-FH waveform used in this research and the assumptions, limitations, and variables placed upon it. Simulation models for both the wideband and channelized radiometers were developed to include discussions on CFAR processing. A delay and intercept receiver model was introduced as an alternative to the radiometric models. The wideband and narrowband jamming transmitters and their associated waveforms were introduced. Chapter 4 provides simulated detection results for a variety of alterations on the signal, intercept receiver, and jamming parameters for both the wideband and channelized radiometer. Chapter 5 presents conclusions drawn from the research and provides recommendations for future research. Appendix A is a compilation of simulations performed using the delay and

multiply receiver developed in Chapter 3 with preliminary results that did not perform well enough to warrant a detailed investigation. Appendix B contains the MATLAB<sup>®</sup> code used in the simulations.

## 2 Background

### 2.1 Introduction

This chapter introduces the method of determining the desired performance parameters in a tactical communication environment. Section 2.2 introduces the typical tactical communication scenario. Section 2.3 discusses the communication link of the scenario to include Low Probability of Intercept signaling techniques and the Gaussian Minimum Shift Keying waveform. Section 2.4 describes the interception link of the scenario to include non-cooperative receiver models. Section 2.5 combines the discussions of the two links and develops a metric for determining the relative performances of the links. Section 2.6 summarizes the chapter.

### 2.2 Tactical Communication Scenario

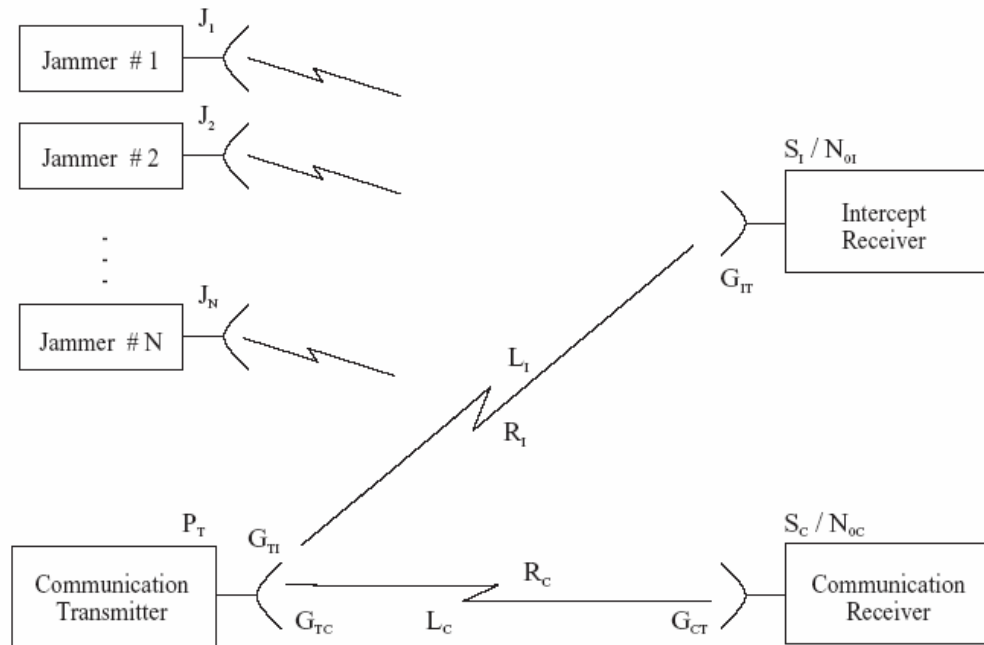


Figure 2.1 Tactical Communication Scenario [3]

A typical tactical communication scenario can be illustrated by Figure 2.1. In this drawing, a communication transmitter is sending a signal to a communication receiver

located a distance  $R_C$  away. The transmitter is using a power designated as  $P_T$  while the receiver receives a signal power of  $S_C$ . In addition to the two communicating devices, there are several jamming transmitters as well as an intercept receiver. The intercept receiver is located at a distance  $R_I$  from the transmitter. The goal of the intercept receiver is to achieve detection goals (probability of detection, probability of false alarm) as far away from the communication receiver as possible to avoid compromising its own position. In addition, once the signal has been detected, the interceptor will make an attempt to exploit the signal's transmitted information, which requires increasingly sophisticated processing techniques. The jamming transmitters are emitting signals that attempt to disrupt the communication link by adding unwanted energy to the communication channel. The intercept receivers are also affected by the jamming signals.

From this scenario two major areas will be discussed in detail: the communications link and the interception link.

### 2.3 Communication Link

Through the use of link budget techniques to include the Friis Path Loss Equation, the received signal power  $S_C$  can be expressed as

$$S_C = \frac{P_T G_{TC} G_{CT}}{(4\pi R_C / \lambda)^2 L_C} \quad (2.1)$$

where

- $G_{TC}$  is the antenna gain in the direction of the receiver
- $G_{CT}$  is the antenna gain in the direction of the transmitter
- $(4\pi R_C / \lambda)^2$  is the free-space propagation loss (assumes air to air is “free space”)

- $\lambda$  is the wavelength of the signal
- $L_C$  is the atmospheric loss factor due to moisture and other effects

Taking the noise power spectral density (PSD) to be  $N_{SC}$ , which is the sum of the additive white Gaussian thermal noise (AWGN) and the jamming signal, the communication signal to noise ratio (signal power to noise PSD) can be expressed as

$$SNR_C = R_b \frac{E_b}{N_{SC}} = \frac{P_T G_{TC} G_{CT}}{L_C N_{SC}} \left( \frac{\lambda}{4\pi R_C} \right)^2 \quad (2.2)$$

where  $E_b$  is the energy per bit and  $R_b$  is the bitrate. Thus, given an  $SNR_C$ ,  $R_C$  can be determined by

$$R_C = \sqrt{\frac{P_T G_{TC} G_{CT}}{L_C N_{SC}} \left( \frac{\lambda}{4\pi} \right)^2 \frac{1}{SNR_C}} \quad (2.3)$$

It becomes apparent that the two key factors above for the communications link are  $R_C$  and  $SNR_C$ . When  $R_C$  is given (i.e., the positions of transmitter and receiver are fixed), the communications link must meet a certain  $SNR_C$  to meet a predetermined performance metric. For most communication links this is a probability of bit error rate (usually expressed as  $P_B$ ). Systems can usually be described by curves such as those presented in Figure 2.2 below. As the  $SNR_C$  of the link increases, the  $P_B$  will decrease in some manner determined by the link itself.

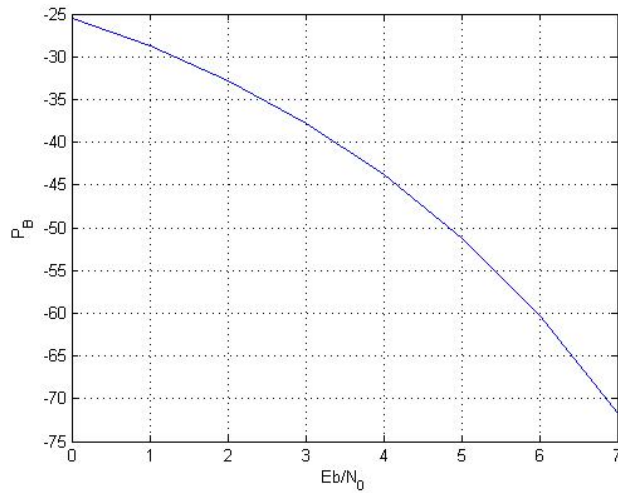


Figure 2.2 Representative Bit Error Curve Plot

The communication link designer would like to reduce the  $SNR_C$  for the given  $P_B$  by as much as possible (equivalent to moving the curve to the left). This can be done through methods such as error correction coding, reducing the bit rate, and using efficient modulation techniques. In this research it is assumed that the  $R_C$  and  $P_B$  are fixed quantities (i.e., the communication system is a known constant). Thus, the  $SNR_C$  required to maintain the  $(P_B, R_C)$  pair is also constant.

**2.3.1 Frequency Hopping (FH).** The communication system designer has other factors to consider besides being able to communicate at a certain range. In the tactical environment shown in Figure 2.1, intercept receivers and jammers are attempting to compromise the link. The intercept receiver will attempt to non-cooperatively detect the signal of interest (SOI) while the jamming transmitters will attempt to “drown-out” the communication signal through RF interference. The communication waveform can be manipulated in such a way to make these tasks more difficult. A field of study known as Low Probability of Intercept (LPI) Communications is devoted to designing waveforms

that make interception and jamming more difficult. One of the most popular and effective techniques is Frequency Hopping (FH).

In FH signals, the signal is transmitted on a certain carrier frequency for a time  $T_2$ . At this time, the carrier frequency will shift (“hop”) to another frequency and stay there for another  $T_2$ , and so on. The number of hops per second is referred to as the hop rate. The communication receiver is synchronized to the transmitter and follows the hopping sequence, whereas an intercept receiver and jammer usually do not. The hopping pattern can be represented graphically in Figure 2.3.

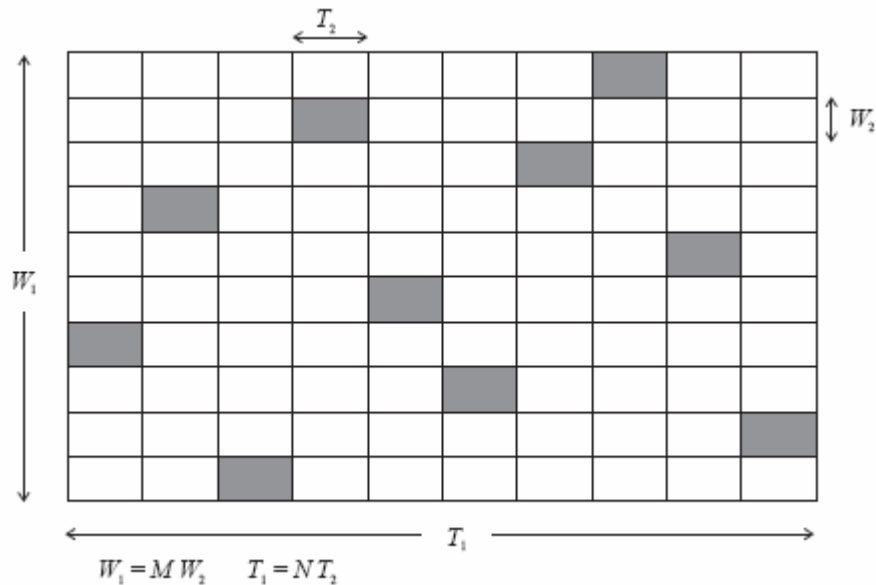


Figure 2.3 FH Signal Space [3]

The signal is said to exist for a time of  $T_1$  seconds with a hop duration of  $T_2$  seconds. As the figure indicates, the number of channels is designated  $M$  while  $N$  is the number of hops in  $T_1$ . Through frequency hopping, the energy of the transmitted signal is effectively “spread” over a BW of  $W_1$ , which is why FH signals are also classified as spread spectrum (SS) signals. An intercept receiver will have to examine the entire signal space instead of just one carrier frequency to observe the entirety of the signal. In



a similar manner, the jamming device, in order to completely disrupt communications, must be able to spread its energy out such that it affects more than just one carrier frequency.

**2.3.2 Gaussian Minimum Shift Keying (GMSK).** The signal waveform itself can be improved for use in mobile and tactical situations. One of the more popular modulation techniques is Gaussian Minimum Shift Keying (GMSK), used in modern systems such as Bluetooth, the Global System for Mobile Communications (GSM), and Tactical Targeting Network Technology (TTNT). It is a modulation scheme that varies the phase of the carrier in accordance with the modulating data. It is a variation of Minimum Shift Keying (MSK) in that a Gaussian filter is used prior to modulation. [4]

**2.3.2.1 MSK.** MSK is a type of phase modulation that does not have phase discontinuities. The continuous phase reduces the bandwidth occupied by the signal in comparison to conventional phase modulation techniques. MSK is superior to Amplitude Shift Keying (ASK) in wireless communications because background noise and environmental factors, affecting the energy level of the signal, will cause direct errors in the energy-dependant ASK demodulation schemes, whereas MSK is much more robust. MSK does have out of band radiation that prevents it from being used in single-channel-per-carrier (SCPC) mobile radio. [4]

**2.3.2.2 GMSK Defined.** To further reduce signal bandwidth (and allow it to be used in SCPC mobile radios), a pre-modulation Gaussian filter is applied. The filter has the form [5]

$$h(t) = \frac{1}{\sqrt{2\pi\sigma T}} \exp\left(\frac{-t^2}{2\sigma^2 T^2}\right), \sigma = \frac{\sqrt{\ln(2)}}{2\pi BT} \quad (2.4)$$

where  $BT$  is the time-bandwidth product of the filter and  $T$  is the duration of the pulse. Approximately 99% of the RF bandwidth is  $2B/T$  Hz. For most mobile radio applications,  $BT=0.3$ , which is the value used in this research.

The shaping pulse is [5]

$$g(t) = \frac{1}{2T} \left[ Q \left( 2\pi BT \frac{t-T/2}{T\sqrt{\ln(2)}} \right) - Q \left( 2\pi BT \frac{t+T/2}{T\sqrt{\ln(2)}} \right) \right] \quad (2.5)$$

where

$$Q(x) = \frac{1}{\sqrt{2\pi}} \int_x^{\infty} \exp(-u^2 / 2) du \quad (2.6)$$

Example pulses are shown in Figure 2.4 below for commonly used values of  $BT$ .

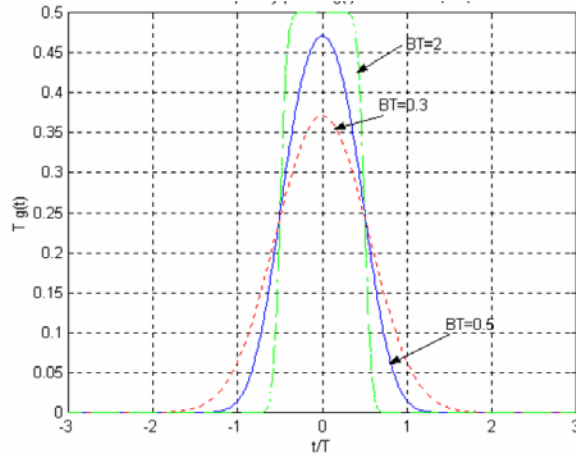


Figure 2.4: GMSK Pulses

The modulated and pulsed signal then becomes

$$s(t) = \sqrt{2E_b T} \cos(2\pi f_c t + \theta(t) + z_0) \quad (2.7)$$

where

$$\theta(t) = \sum_i m_i \pi h \int_{-\infty}^{t-iT} g(u) du \quad (2.8)$$

$m_i$  is the NRZ stream of data,  $z_0$  is the initial phase,  $E_b$  is the energy of the signal,  $h$  is the modulation index of the signal (0.5 for this research, which means each subsequent input bit will cause a phase change of  $h$  radians), and  $f_c$  is the carrier frequency. Figure 2.5 is a time-domain plot of a sample GMSK signal with a duration of two bits that looks very similar to any RF signal. Figure 2.6 is a plot of the NRZ input bitstream and the associated carrier phase ( $\theta(t)$  in (2.8)). The smoothly varying phase changes, are significantly different that the abruptness of classic PSK modulation techniques. Figure 2.7 illustrates the difference in bandwidth between a common binary phase-shift keyed (BPSK) signal and a GMSK signal using the same modulating data.

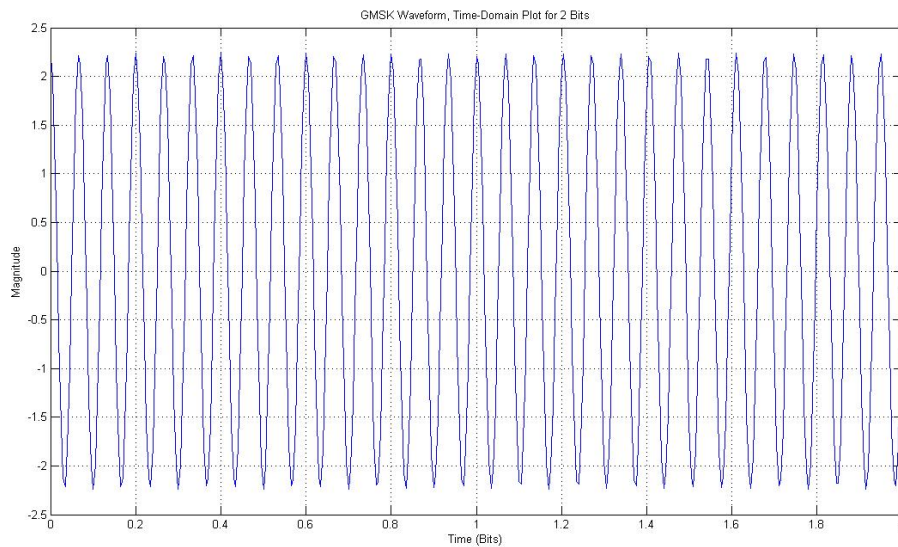


Figure 2.5 Time Domain Plot of GMSK Signal

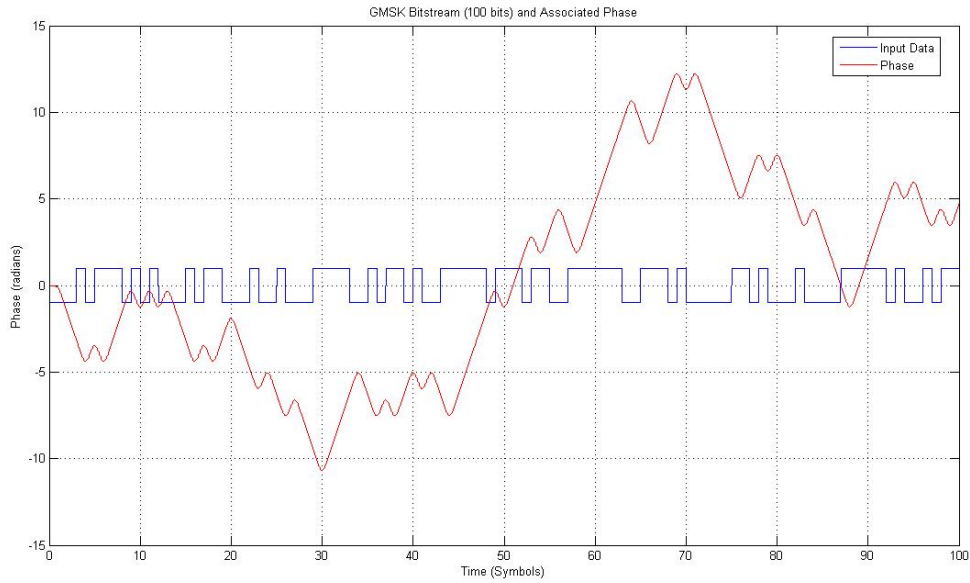


Figure 2.6 Input Data vs. Phase, GMSK Modulation

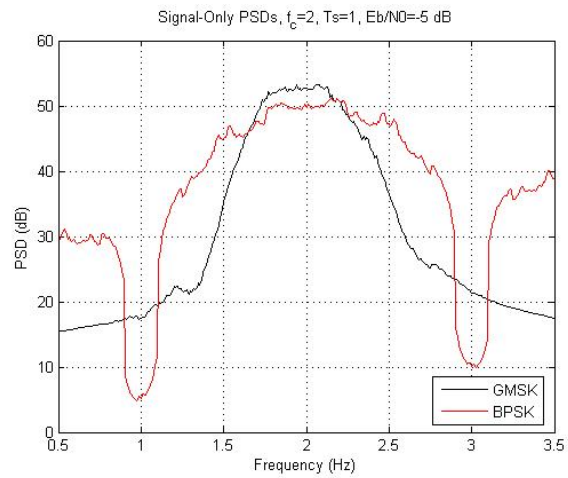


Figure 2.7: Simulated PSDs of BPSK and GMSK

## 2.4 Interception Link

Following the same procedure used for the communications link,

$$S_I = \frac{P_T G_{TI} G_{IT}}{(4\pi R_I / \lambda)^2 L_I} \quad (2.9)$$

where

- $G_{TI}$  is the antenna gain in the direction of the intercept receiver
- $G_{IT}$  is the antenna gain in the direction of the transmitter
- $(4\pi R_I / \lambda)^2$  is the free-space propagation loss
- $\lambda$  is the wavelength of the signal
- $L_I$  is the atmospheric loss factor due to moisture and other factors

Taking the interference link noise PSD to be  $N_{SI}$ , the interception signal to noise ratio can be expressed as

$$SNR_I = R_b \frac{E_b}{N_{SI}} = \frac{P_T G_{TI} G_{IT}}{L_I N_{SI}} \left( \frac{\lambda}{4\pi R_I} \right)^2 \quad (2.10)$$

Thus, given an  $SNR_I$ , the associated intercept range  $R_I$  can be determined by

$$R_I = \sqrt{\frac{P_T G_{TI} G_{IT}}{L_I N_{SI}} \left( \frac{\lambda}{4\pi} \right)^2 \frac{1}{SNR_I}} \quad (2.11)$$

This equation indicates that increasing the antenna gains, increasing the transmitted signal power, increasing the wavelength of the signal, reducing the path loss, and reducing the SNR of the link will all increase the distance the intercept receiver can be from the communication transmitter to achieve a desired probability of detection ( $P_D$ ) and probability of false alarm ( $P_{FA}$ ). However, the intercept receiver cannot control the transmitted power, the transmitter's antenna gain, the path loss, or the wavelength of the signal. For the purposes of this research, the intercept receiver's antenna gain is held

constant since the focus is on the processing techniques rather than the equipment. Thus, (2.11) can be manipulated such that the incremental change in range is

$$\Delta R_I \sim \sqrt{\frac{1}{\Delta SNR_I}} \quad (2.12)$$

which indicates that the receiver would like to decrease its required SNR for the given performance parameter.

As stated in the preceding sections, the performance parameter for the communications link was the probability of bit error. Similarly, the performance parameter for the intercept receiver is the  $P_D$  for a given  $P_{FA}$ . The  $P_D$  is the probability that the signal will be accurately detected whereas the  $P_{FA}$  is the probability that the signal will be declared present when it is in fact absent.

To achieve a certain ( $P_D$ ,  $P_{FA}$ ) pair, a specific SNR is required (the same  $SNR_I$  that appears in (2.12) and earlier). This SNR can be changed through a variety of intercept receiver techniques using non-cooperative detection.

**2.4.1 Non-Cooperative Detection Overview.** When the signals in the environment are not known, it becomes necessary to use non-cooperative detection techniques (as opposed to the ideal matched-filter technique). These receivers sample the environment, apply various processing techniques, and generate a test statistic  $Z$ . This test statistic is then compared to a threshold  $Z_T$  that is established using classic detection criteria (Neyman-Pearson, Minimax, Bayes, etc.) [6]. If the test statistic exceeds the threshold, the signal of interest (SOI) is declared present. The probability of detection ( $P_D$ ) is the probability that the SOI will be declared present if it is actually present, while the probability of false alarm ( $P_{FA}$ ) is the probability that the SOI will be declared present if the channel is noise-only (noise here refers to both thermal noise and any

jamming/interference that may be present). The threshold can typically be adjusted such that a constant false alarm rate (CFAR) can be achieved. The following sections discuss the wideband and channelized radiometers.

**2.4.2 Wideband Radiometer.** The classic wideband radiometer (the most basic form of energy detection) estimates the energy received in a bandwidth  $W$  over an observation time of  $T$ . With prior knowledge about the SOI,  $W$  and  $T$  can be scaled to cover the signal space in such a way to minimize noise-only samples. The wideband radiometer has the following block diagram:

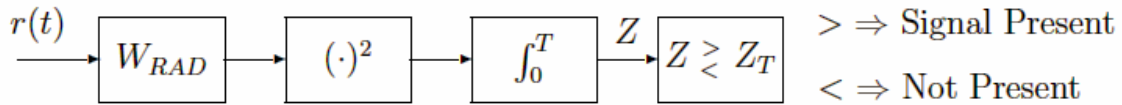


Figure 2.8: Wideband Radiometer Block Diagram [3]

The received signal  $r(t)$  is passed through a bandpass filter with a bandwidth of  $W$  Hz. The filtered signal is squared and then integrated for  $T$  seconds. The output of the integration is the test statistic  $Z$ , which is then compared to the threshold  $Z_T$ . If  $Z > Z_T$ , the signal is declared present. If not, it is assumed to be absent. If the input to the radiometer is strictly AWGN, the normalized test statistic  $2Z/N_0$  has a chi-square probability density function (PDF) with  $2TW$  degrees of freedom. Similarly, if a signal is present, the normalized test statistic has a non-central chi-square PDF with  $2TW$  degrees of freedom and a non-centrality parameter  $2E/N_0$ , where  $E$  is the energy of the signal measured over  $T$  seconds. Example PDFs are shown in Figure 2.9.

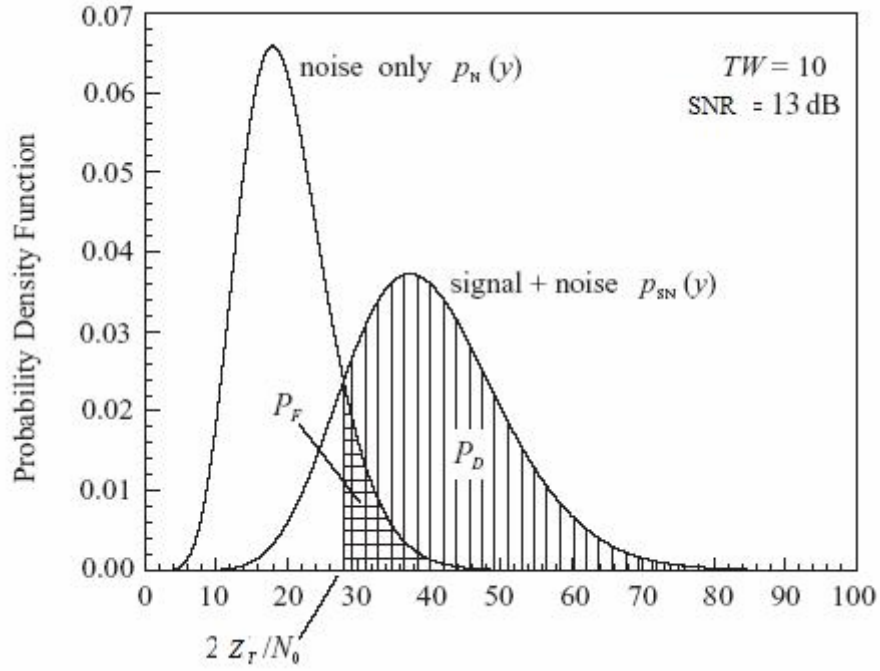


Figure 2.9 Chi-Square PDFs of Noise and Signal Plus Noise [3]

For the normalized decision threshold  $2Z_T / N_0$ ,  $P_D$  and  $P_{FA}$  are defined by the following:

$$P_D = \int_{2Z_T / N_0}^{\infty} p_{sn}(y) dy \quad (2.13)$$

$$P_{FA} = \int_{2Z_T / N_0}^{\infty} p_n(y) dy \quad (2.14)$$

where  $p_{sn}(y)$  is the PDF of the signal plus noise and  $p_n(y)$  is the PDF of the noise only case. The signal plus noise PDF in Figure 2.9 is located to the right of the noise-only PDF as it contains more energy. The shaded areas to the right of the threshold indicate  $P_{FA}$  and  $P_D$ . The separation between the two PDFs is directly related to the SNR. If the SNR increases through increasing the signal energy (with the noise floor remaining constant), the signal plus noise PDF will move to the rights while the noise PDF will



remain stationary. Hence, if the threshold were to remain the same,  $P_D$  will increase while  $P_{FA}$  will remain the same.

Given a desired  $P_D$  and  $P_{FA}$  (typically specified by mission objectives), the required signal to noise ratio ( $SNR_{req}$ ) can be solved using (2.13) and (2.14), but they are not in closed form. To alleviate this problem, many models have been developed to estimate the  $SNR_{req}$  within 0.5 dB for  $TW > 1000$  as shown in [6]. One of the simpler models is Edell's model, which is given as

$$SNR_{req} = d\sqrt{W/T} \quad (2.15)$$

where

$$d = Q^{-1}(P_{FA}) - Q^{-1}(P_D) \quad (2.16)$$

$Q^{-1}(x)$  is the inverse of the function given in (2.6). This model is reported to be accurate to approximately 0.3 dB for a  $TW$  of 1000 and 0 dB as  $TW \rightarrow \infty$ . If  $TW$  is small ( $TW < 100$ ), other models may provide greater accuracy. One such model (used in the theoretical results portion of this research) is Engler's model given by

$$SNR_{req} = \left( X_0 + \sqrt{X_0^2 + 16TWX_0} \right) / 4T \quad (2.17)$$

where  $X_0 = d^2$  in (2.14). Engler's model is accurate to within 0.5 dB for  $TW < 100$ , which becomes 0 dB with  $TW > 1000$ , at which point it reduces to Edell's model.

(2.15) and (2.17) contain very important implications. Since  $d$  is the degree of separation between the PDFs, as  $d$  increases  $SNR_{req}$  increases, which is the converse of the explanation of Figure 2.9 given above. As the bandwidth  $W$  increases, the  $SNR_{req}$  increases. This is due to the fact that the bandpass filter is admitting more noise as it becomes wider while the amount of signal remains relatively constant. As a result, to achieve the same  $(P_D, P_{FA})$  pair, the signal energy must increase. Finally, an increase in

$T$  will decrease  $SNR_{req}$ . This is due to the time-averaging property of integration. Since the background noise is largely uncorrelated, it will average out to zero, whereas the signal, which is highly correlated, will not. Thus, a lower SNR is required to maintain the same performance requirements.

**2.4.3 Channelized Radiometer.** The wideband radiometer is useful when very little information is known about the signal, but it is also subject to relatively poor performance due to the large amount of noise in the system introduced by its large bandwidth. If the SOI is a frequency hopped (FH) signal in which the bandwidth of each channel ( $W_2$ ) is much less than the bandwidth of the entire signal space ( $W_1$ ), a channelized radiometer may be employed. Figure 2.3 illustrated a typical signal space occupied by a FH signal. If the interception receiver has prior knowledge of  $W_2$  and  $T_2$ , a channelized radiometer can be used to enhance detection performance over the wideband radiometer.

In a classic channelized radiometer, energy detection techniques are used on each individual cell of Figure 2.3 and a soft decision is made in each  $W_2 \times T_2$  cell. The aggregate decisions are then used to make a final present/not present decision. The channelized radiometer has the following block diagram:

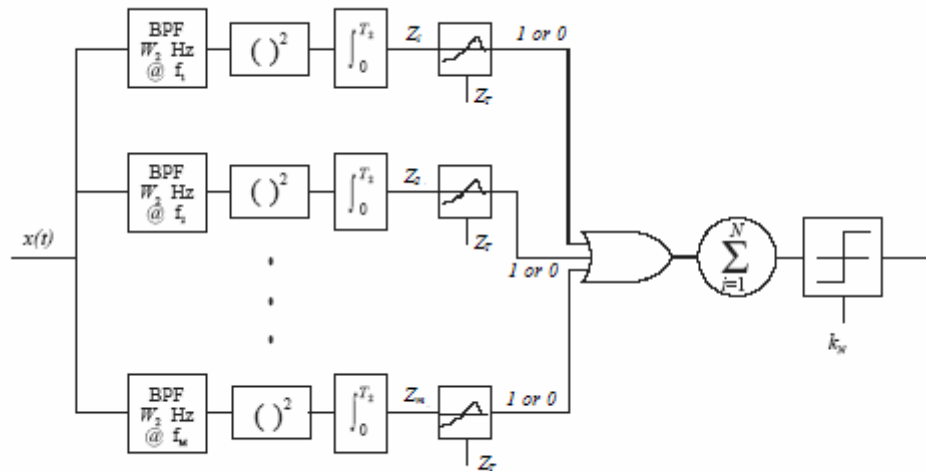


Figure 2.10 Channelized Radiometer Block Diagram (Binary-OR) [3]

The received signal is partitioned via  $M$  bandpass filters with bandwidths of  $W_2$ . Each of the filtered outputs are squared and integrated over  $T_2$ . The outputs ( $Z_m$ ) are compared to  $Z_T$  to create  $M$  detection decisions. If at least one detection in  $M$  channels is declared, a “1” is stored for that particular hop interval. After the process has repeated  $N$  times (covering the entire  $T_1$ ), the accumulation of per-hop detections  $k$  is compared against a second threshold  $k_N$  set at a constant value that is a fraction of  $N$ . Experiments have shown [7] that  $0.6N$  is a reliable figure to use for  $k_N$ . If  $k > k_N$ , the signal is declared present for the entire signal space. An assumption has been made that there will be no more than one signal present in the environment. Thus, an OR-gate is used at the output of the cell thresholding process to determine if the signal is present in the  $W_i \times T_2$  space under investigation. Hence, the model presented is often called the Binary-OR Channelized Radiometer [7]. However, other techniques have been proposed that are as accurate as the Binary-OR but require slightly less processing [8].

Much like the wideband radiometer, the channelized radiometer has well-established equations that can calculate a required SNR given  $P_D$  and  $P_{FA}$ . However, since there are two decisions involved, the calculations are iterative in nature. For the following equations,  $Q_F$  refers to the per-cell probability of false alarm and  $Q_D$  refers to the per-cell probability of detection, while  $P_{FA}$  and  $P_D$  retain their overall probability definitions.

The overall  $P_{FA}$  is the probability that  $k_N$  or more hop decisions result in a detection when no signal is actually present (the energy received is strictly noise-only). The probability that none of the  $M$  channels has a false alarm is the product of the probabilities of each cell not having a false alarm,  $(1 - Q_F)^M$ . Thus, the probability of a “1” at the output of the OR gate in the noise-only case will be the probability that at least one of the channels has a false alarm, expressed as:

$$p_0 = 1 - (1 - Q_F)^M \quad (2.18)$$

which assumes that the noise processes in each channel are independent. The probability this occurs exactly  $i$  out of the  $N$  times will be  $\binom{N}{i} p_0^i (1 - p_0)^{N-i}$ , via the binomial expansion theorem. Thus, the  $P_{FA}$  will be the summation of the probabilities of all possible events exceeding the  $k_N$  hop-count threshold:

$$P_{FA} = \sum_{i=k_N}^N \binom{N}{i} p_0^i (1 - p_0)^{N-i} \quad (2.19)$$

In the signal plus noise case, the probability of a “1” at the output of the OR gate will be the probability of a single detection or at least one false alarm. This can be

expressed as one minus the probability of a missed detection and  $M-1$  missed false alarms,

$$p_1 = 1 - (1 - Q_D)(1 - Q_F)^{M-1} \quad (2.20)$$

Therefore, using the same binomial expansion procedure as with the noise-only false alarm case, the signal plus noise detection case can be expressed as:

$$P_D = \sum_{i=k_N}^N \binom{N}{i} p_1^i (1 - p_1)^{N-i} \quad (2.21)$$

Given  $P_{FA}$  and  $P_D$ ,  $p_0$  and  $p_1$  can be solved using (2.18) and (2.20). Thus,

$$Q_F = 1 - (1 - p_0)^{1/M} \quad (2.22)$$

$$Q_D = 1 - \frac{1 - p_1}{(1 - Q_F)^{M-1}} \quad (2.23)$$

and (2.15) and (2.17) can be used to solve for  $SNR_{req}$ , with  $W_2$  and  $T_2$  used in place of  $W$  and  $T$  and  $Q_F$  and  $Q_D$  used in place of  $P_{FA}$  and  $P_D$ .  $SNR_{req}$  is the same as  $SNR_I$  in the equations presented earlier (2.10). The interceptor would like this to be as small as possible for a given  $P_D$  and  $P_{FA}$ , and ideally it would be smaller than the equivalent  $SNR_I$  for a wideband radiometer with the same  $W_I$  and  $T_I$  parameters. The same conclusions can be drawn from the channelized equations as the wideband equations (increasing  $T_2$ , reducing  $W_2$ , and increasing  $d$  all improve performance), but the results are not as immediately discernable due to the iterative process of solving the equations.

The channelized radiometer is clearly more complicated than the wideband radiometer (and hence more difficult to implement), but the rewards are generally twofold: an increase in waveform detectability (under certain conditions, as given in Chapter 4) and an increase in post-detection processing flexibility necessary for further

signal exploitation. For example, the channelized radiometer has the ability to differentiate between two adjacent signals using a short-time Fourier Transform (STFT) [9] whereas the wideband radiometer does not. Thus, with  $R_C$  and  $R_I$  fixed, the communication waveform designer would like to force the interceptor to use a radiometer for detection, which will occur when  $SNR_I$  is higher for a channelized radiometer than a wideband radiometer.

## 2.5 Quality Factors

Earlier in this chapter the communication and interception links were discussed separately. Methods to reduce  $SNR_C$  and  $SNR_I$  were discussed as well as the performance metrics of both systems. With  $SNR_C$  and  $SNR_I$  given, the following expression can be derived from (2.3) and (2.11):

$$\left(\frac{R_C}{R_I}\right)^2 = \frac{G_{CT}G_{TC}}{G_{IT}G_{TI}} \frac{L_I}{L_C} \frac{N_{SI}}{N_{SC}} \frac{SNR_I}{SNR_C} \quad (2.24)$$

This is known as the LPI Equation [3]. From the previous discussion it is clear that the communication system would like to increase this ratio whereas the interceptor would like to decrease it. (2.24) can be broken down into smaller expressions known as Quality Factors that analyze one particular aspect of the environment, such as the Antenna Quality Factor ( $G_{CT}G_{TC}/G_{IT}G_{TI}$ ), Atmospheric Quality Factor ( $L_I/L_C$ ), and Interference Suppression Quality Factor ( $N_{SI}/N_{SC}$ ). However, as stated earlier this research assumes all the quantities on the right side of (2.24) are fixed with the exception of the SNRs, reducing it to the Modulation Quality Factor ( $Q_{MOD}$ ), expressed as [3]

$$Q_{MOD} = 10 \log \left( \frac{SNR_I}{SNR_C} \right) \quad (2.25)$$

The intercepting receiver desires a small  $Q_{MOD}$ , which requires the  $SNR_I$  to be low relative to the  $SNR_C$ . In this research, since the communication link is assumed to have a constant  $SNR_C$  regardless of the scenario, the sole parameter as far as optimization is concerned is  $SNR_I$ , which can be altered either through different receiver techniques, signal parameters, or the presence of jamming.

For each scenario tested, there will be a unique  $SNR_I$  for each intercept receiver tested, creating an  $SNR_W$  for the wideband radiometer and an  $SNR_{Ch}$  for the channelized radiometer. Since the intercept receiver would prefer to have the channelized radiometer outperform the wideband radiometer, another metric is introduced to test the relative merits of both, namely the Intercept Quality Factor, expressed as

$$Q_{INT} = 10 \log \left( \frac{SNR_W}{SNR_{Ch}} \right) \quad (2.26)$$

From the interceptor's point of view, for a given  $(P_{FA}, P_D)$  the channelized radiometer would outperform the wideband radiometer when  $SNR_W$  is greater than  $SNR_{Ch}$ . Thus, the larger the  $Q_{INT}$ , the more effective the channelized radiometer is versus wideband radiometer. The goal of the intercept receiver is to maximize this as much as possible, since the channelized detector is more preferable.

## 2.6 Summary

This chapter introduced the communication/interception scenario to include discussions on both the communication and interception links. The Frequency Hopping and Gaussian Minimum Shift Keying techniques were also introduced in this chapter. Non-cooperative detection schemes commonly used for frequency hopped signals,

specifically the wideband and channelized radiometers, were discussed. Functional diagrams and equations governing the two techniques were presented and discussed, with particular emphasis placed on obtaining a required signal to noise ratio from a given probability of false alarm and probability of detection. Quality Factor calculations for the scenario were developed under the assumption that the communication link metrics remain constant. Methods for simulating these and related intercept receivers will be presented in Chapter 3, along with the simulations of the signal of interest and jamming transmitters.



### 3. Methodology

#### 3.1 Introduction

This chapter discusses the simulations used for this research to include the construction of the signal and intercept receivers. Section 3.2 describes the signal parameters used in this research. Section 3.3 discusses the simulation of the various radiometric detection techniques. Section 3.4 introduces the delay-and-multiply intercept receiver. Section 3.5 examines the jamming transmitters. Section 3.6 summarizes the chapter.

#### 3.2 Signal Structure

The simulated signal used in this research is tangentially modeled after the Tactical Targeting Network Technology (TTNT) waveform being developed for airborne datalink communications. For the scope of this research, the most basic parameters of the signal in question are analyzed while the analysis of the specific signal is left for later research.

**3.2.1 Signal Generation.** Section 2.3.2 of this thesis described the theoretical development of the GMSK signal. To simulate this signal, the quadrature model is used as shown in Figure 3.1.

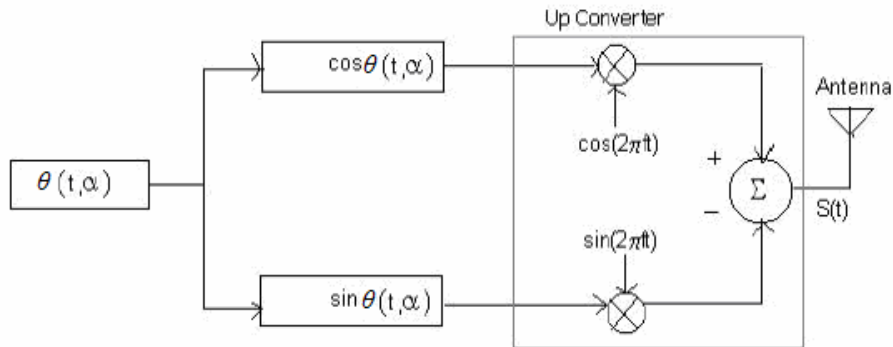


Figure 3.1 GMSK Generation Block Diagram

The input phase is determined from (2.8).

**3.2.2 Signal Parameters.** The signal simulated in this research used parameters that are representative of those used in the TTNT waveform. The numbers used for the simulated signal were chosen because of their ease of use and manipulation in the simulation programming. However, these numbers can be scaled by a common factor to approximate the TTNT's parameters. The following assumptions and limitations were used in the generation of the signal of interest:

- The observed signal consists of a frequency-hopped pulse between 40 and 96 bits long. The bit rate ( $R_b$ ) will be 1 bit/second, thus  $T_l$  will be between 40 and 96 seconds. The TTNT signal has a default bit rate of 2 Mbps and a duration of 20-54  $\mu$ sec, thus when scaled to 1 bps the duration is 40-108 bits (96 was used because of scaling factors).
- The signal has a default hop rate of 1/8 hops/second, giving a hop period of 8 seconds/hop. The hop rate can be varied.
- The modulation scheme is GMSK with  $BT=0.3$  and  $h=0.5$ .
- There are  $M=15$  channels from 2 Hz to 30 Hz evenly spaced by 2 Hz (2 Hz, 4 Hz, 6 Hz, etc.). Since the simulated  $R_b$  is 1 bps and the null-to-null bandwidth of a BPSK modulated waveform is  $2/R_b$  Hz [14], the bandwidth of each channel in the simulation becomes 2 Hz. They are spaced 2 Hz apart to mitigate adjacent channel interference. 15 channels are used because the TTNT waveform uses 15 channels. The number of channels cannot change. The TTNT waveform's frequencies are between 1.358 GHz to 1.841 GHz with 13.3 MHz between channels, which is larger than the 4 MHz equivalent simulated in this research.

- The signal as a default exists for the entire duration of the pulse, but jitter is allowed in which the signal will only exist for a certain percentage of the time.

In addition to the assumptions about the signal, it is also assumed that the background is stationary additive white Gaussian noise (AWGN).

**3.2.3 Intentional Jitter.** A key signal parameter is its ability to introduce intentional jitter to increase its LPI performance. For this research, jitter is defined as the amount of compression the signal undergoes per hop. For instance, the signal typically exists for a duration of  $T_2$  seconds per hop. With a jitter of  $J$ , the signal is compressed in time such that it exists for  $T_2 - JT_2 = (1 - J)T_2$  seconds per hop with a delay (noise-only duration) of  $JT_2$  seconds. In a real system, the compressed signal is then shifted by a random amount within the original  $T_2$ . However, since the intercept receivers examined in this research are unable to track the shifting signal and rely exclusively on the total amount of energy within  $T_2$ , the jittered signal is modeled to exist for the first  $(1 - J)T_2$  of the  $T_2$  cell.

### 3.3 Intercept Receiver Processing

The intercept receivers simulated in this research use ideal square filters. In the cases in which CFAR processing is used a CFAR of 0.01 has been implemented to establish a baseline for comparison between the receiver models. In an actual system, the CFAR will usually be much less (on the order of  $10^{-5}$ ). The reduced CFAR is implemented in the simulation because it drastically reduces simulation time while preserving a conceptual framework. However, this research focuses on relative effects and is not primarily concerned with real-world results. Each simulation that yields a test

statistic is repeated 10,000 times in order to achieve an appropriate number of false alarms (100) to yield reliable results.

**3.3.1 Wideband Radiometer.** The wideband radiometer has been selected as the baseline detection scheme because it is the simplest receiver and requires the least amount of knowledge regarding the signal. The wideband radiometer has *a priori* knowledge of  $W_I$  and  $T_I$ , but does not care about the number of channels or the number of hops. The simulated wideband radiometer takes a signal of duration  $T_I$  and performs an FFT on it. This spectral information is truncated from 1 to 31 Hz, covering  $W_I$  (which does not change throughout the research). The truncation of the spectral plot is in essence an ideal bandpass filter. Each frequency component is then squared and added to compute the signal test statistic  $Z_S$ . Through the use of Parseval's Theorem of the Fourier Transform, the integration in the frequency domain is equivalent to the integration in the time domain as presented in the models developed in Chapter 2. This process is used for both the signal plus noise and noise-only cases (the same noise vector is used for both for each Monte Carlo trial). The noise-only case will yield  $Z_N$ . The process is outlined in the diagram below:

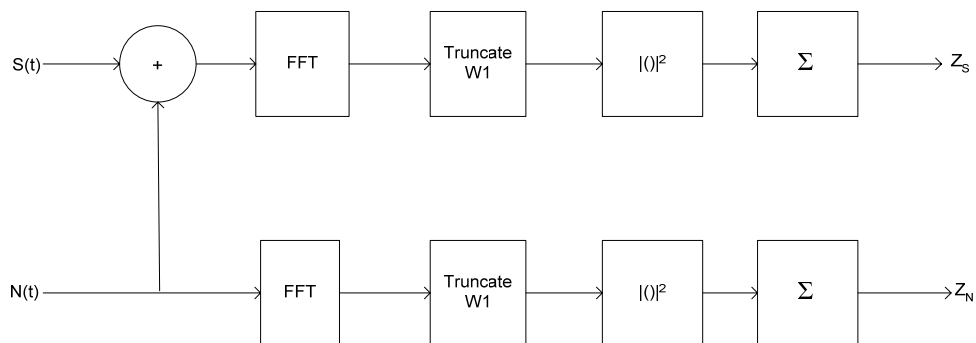


Figure 3.2 Simulated Wideband Radiometer Block Diagram

The threshold  $Z_T$  is determined using CFAR processing in order to obtain meaningful results. After the process as shown in Figure 3.2 has been performed an arbitrarily large number of times (in this case 10,000), the following histogram can be generated using the values of  $Z_N$  and  $Z_S$  for an SNR of 5 dB.

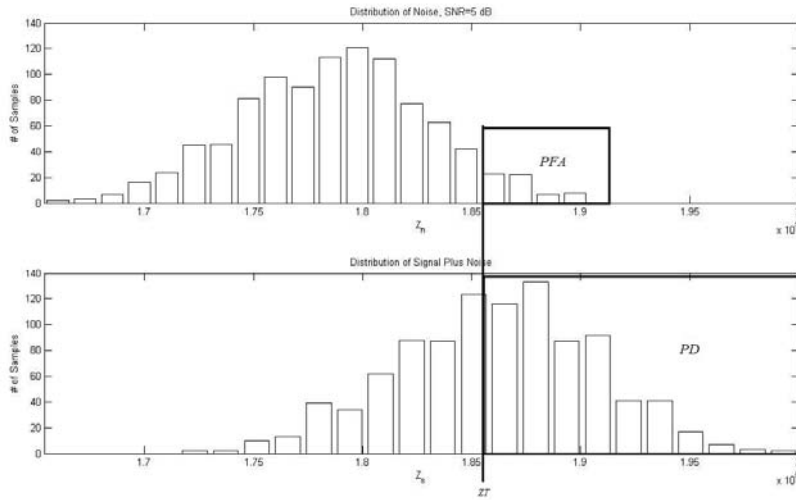


Figure 3.3 Sample Statistics Used for Thresholding

The top histogram is for the noise-only case while the bottom histogram is for the signal plus noise case.  $Z_T$  is the point along the  $Z_N$  axis at which the number of samples to the right equals the number of false alarms required to generate the required  $P_{FA}$ . Thus, for a  $P_{FA}$  of 0.01 and a sample space of 1000, there will be a total of 100 samples to the right of  $Z_N=Z_T$ .  $Z_T$  is then projected down to the signal plus noise histogram. The percentage of signal plus noise samples to the right of  $Z_S=Z_T$  is then the  $P_D$ . Thus, if 75% of the signal plus noise samples are to the right of  $Z_T$ , the  $P_D$  is 0.75 for the  $P_{FA}$  of 0.01.

The figure below is a plot of the simulated wideband radiometer model vs. the theoretical wideband radiometer as calculated through the equations in Chapter 2. The simulated curve is shown to be about 1.5 dB different than the theoretical curve, which is significantly greater than the 0.5 dB theoretical difference given in Chapter 2. Thus, for

the remainder of the research, the analytical model will be used to generate statistics for the wideband radiometer.

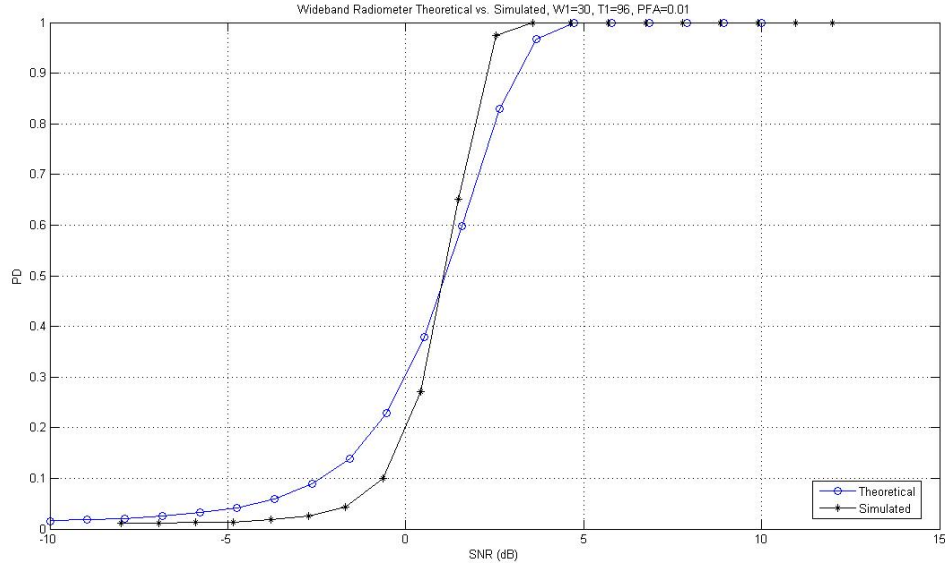


Figure 3.4 Wideband Radiometer, Theoretical vs. Simulated

**3.3.2 Channelized Radiometer.** The simulated channelized radiometer assumes more *a priori* knowledge about the signal than the wideband radiometer. As a result, the channelized radiometer is more flexible in its potential ability to classify and differentiate between signals if the situation allows it. Thus, the intercepting party would like to be able to use a channelized radiometer as opposed to a wideband radiometer. However, it may not always be the optimal choice (in terms of  $Q_{MOD}$ ) for the given situation.

The channelized radiometer has information regarding  $W_1$ ,  $T_1$ , the hoprate (used to determine  $T_2$ ), and the number of channels (used to determine  $W_2$ ). As a baseline, the channelized radiometer uses 15 channels with a  $W_2$  of 2 Hz in order to have complete coverage of  $W_1$  (as the results will show this is not always optimal). The processing of the channelized radiometer essentially divides the signal space up into a grid of  $W_2 \times T_2$  cells as shown in Figure 2.3. Within each cell the wideband processing shown in Figure

3.2 is repeated, except the signal is truncated in time prior to the FFT. The output test statistics  $Z_N$  and  $Z_S$  are intermediate in the case of the channelized radiometer.  $Z_N$  and  $Z_S$  are then compared to a threshold  $Z_T$  and if the signal is declared present, a “1” is designated for that particular cell. If not, the cell is designated “0”. The cell designators are then summed across the  $M$  channels and if the number is greater than or equal to 1, the signal is said to be present for that  $T_2$  and the entire  $W_1 \times T_2$  space is given a “1” or “0”. When the entire signal space has been examined, these  $N$  values are summed, and this final value ( $Z_{NF}$  or  $Z_{SF}$ ) is compared to  $0.6 \cdot N$ , the threshold designated as  $k_N$  as described in Chapter 2. This process is illustrated in Figure 3.5.

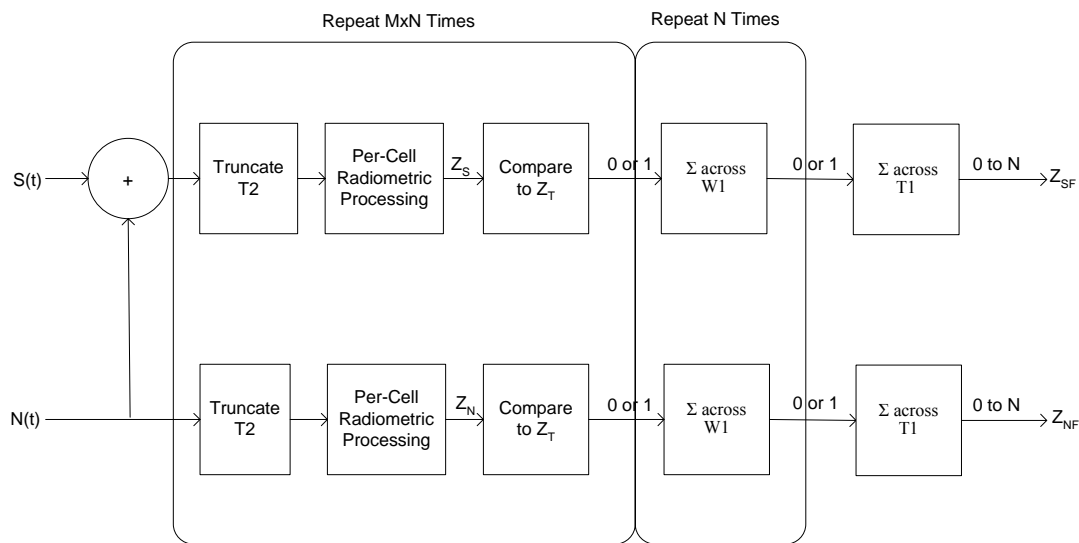


Figure 3.5 Simulated Channelized Block Diagram

The CFAR processing technique is much more complicated in the channelized radiometer than the wideband radiometer. The process for the wideband radiometer cannot be duplicated because the final test statistics out of the channelized radiometer are discrete values (strictly integers from 0 to  $N$ ) that are far too coarse to yield precise results. The threshold must be set at the cell level where  $Z_N$  and  $Z_S$  are generated.

However,  $P_{FA}$  is meaningless in the intermediate stage because  $Q_F$  is the dominant statistic as described in Chapter 2.

Obtaining the proper  $Z_T$  becomes a multi-step process. First, the theoretical models presented in Chapter 2 are used to determine the  $Q_F$  that will deliver the corresponding  $P_{FA}$  with all other factors constant. With a working  $Q_F$ , the wideband radiometer simulation is used with the time and frequency parameters changes to  $T_2$  and  $W_2$  in order to simulate the processing of one cell. With the noise level constant, the process in Figure 3.2 is repeated for various threshold levels. This is repeated until the desired wideband  $P_{FA}$  (actually the channelized  $Q_F$ ) has been achieved. The  $Z_T$  at which this occurs will be used in the channelized radiometer model.

Unlike the wideband  $P_{FA}$  that was simply a percentage of the number of samples and always equal to the desired  $P_{FA}$ , the channelized  $P_{FA}$  will not be exactly the same for each trial due to statistical variations. The accuracy of the estimated  $P_{FA}$  ( $\hat{P}_{FA}$ ) approaches the intended  $P_{FA}$  as the number of trials  $n \rightarrow \infty$ . There is a value  $n_x$  for which any  $n > n_x$  will yield a  $\hat{P}_{FA} \approx P_{FA}$  within a designated standard deviation of  $\sigma$ .

A comparison between the simulated and theoretical channelized radiometers can be seen in Figure 3.5 below. The figure indicates a very strong correlation between the simulated and theoretical plots, differing by no more than 0.3 dB.



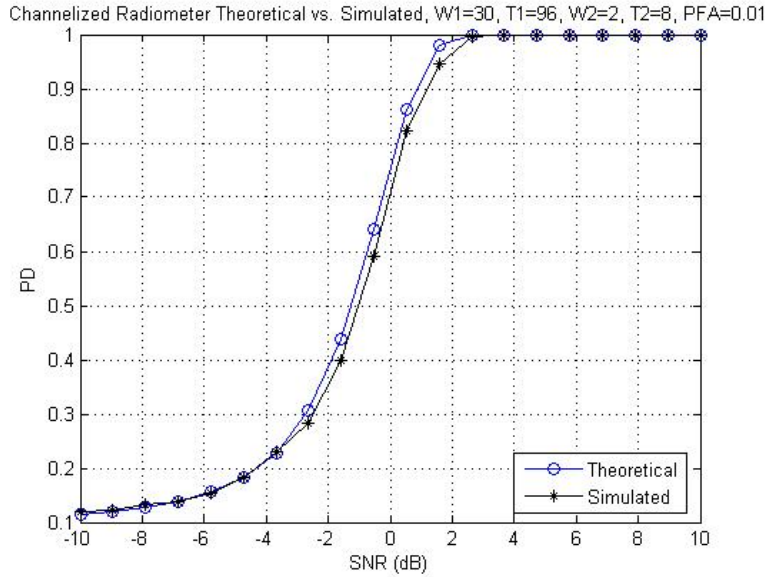


Figure 3.6 Channelized Radiometer: Theoretical vs. Simulated

**3.3.2.1 Narrow Bandwidth Channelized Radiometer.** The channelized radiometer as presented above has been designed such that  $W_2 \times M = W_1$ . This is not a concrete rule because gaps between receiver channels may be allowed exist. These gaps can be beneficial if they consist mostly of noise, which is the case when dealing with the simulated GMSK waveform. As discussed in Chapter 2 and illustrated in Figure 2.7 the bandwidth of the GMSK signal is less than that of a BPSK signal, making it more spectrally compact. Thus, the narrow-bandwidth channelized radiometer reduces  $W_2$  to the 3 dB bandwidth of the signal, which in this case is 0.3 Hz. The limiting factor is in the FFT operation of the channelized radiometer, because a sufficient number of samples must be obtained in the time-truncation step in order to provide the spectral truncation sufficient resolution. In this particular research, the FFT limitation necessitated a  $W_2$  of 0.5 Hz to be simulated.

**3.3.2.2 Sweeping Channelized Radiometer.** The standard channelized radiometer as presented above may not be always available due to practical

considerations. One such problem often encountered is a hardware limitation concerning the number of channels that can be processed at one time, which becomes more pronounced when the number of channels is large. One practical solution is the sweeping channelized radiometer [10].

In the sweeping channelized radiometer, a smaller number of channels each with bandwidth  $W_2$  are grouped together such that they sweep over the entire  $W_1$  space, but not all  $W_1$  can be covered in  $T_2$ . The basic operation is illustrated in Figure 3.7.

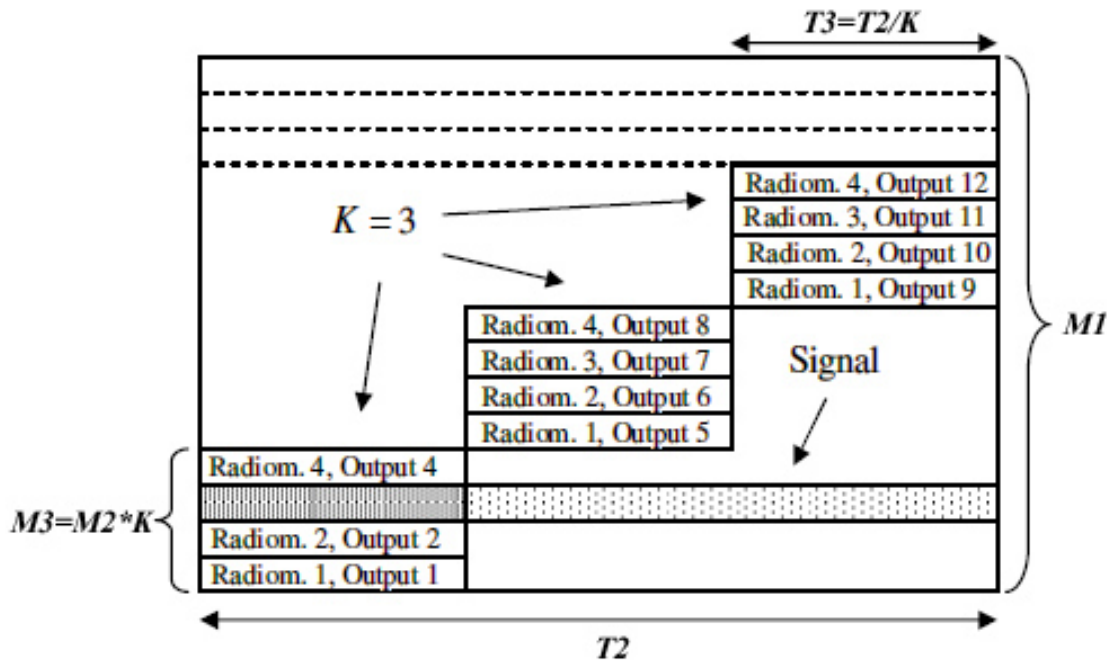


Figure 3.7 Sweeping Channelized Radiometer [10]

In a fast-sweeping channelized radiometer, the group of channels is able to sweep fast enough to cover the entire  $W_1$  in  $T_2$ , but only a fraction of  $T_2$  (designated  $T_3$ ) is integrated at once. If there are  $K$  sweeps per hop as the illustration above shows, then  $T_3 = T_2/K$ . The result is degradation from the channelized radiometer.

An alternative method is a slow-sweep channelized radiometer. In the slow case, the channels will integrate over an entire  $T_2$  ( $T_3=T_2$  in this case) and then hop to the next set of frequencies. The advantage is that the entire  $T_2$  is integrated, but at the same time only  $W_1/K$  can be covered at once, which inevitably leads to part of the signal being missed by the radiometer with a miss probability of  $1-(1/K)$ .

It was shown in [10] that the sweeping channelized radiometer achieves better performance results using maximum based vs. the binary OR processing used in the standard channelized radiometer. In maximum-based processing,  $Z_N$  and  $Z_S$  are not converted to 1s and 0s. After the  $M$  cells within  $T_2$  has been processed, the maximum statistic is retained and compared to a threshold  $Z_T$ , which then establishes a 1 or 0 for the entire  $T_2$ . The rest of the processing is identical to the standard channelized radiometer. A block diagram of the fast-sweeping channelized radiometer is shown below, taking  $K$  in this case to be the number of hops per  $T_2$  (i.e.,  $T_3K=T_2$ ).

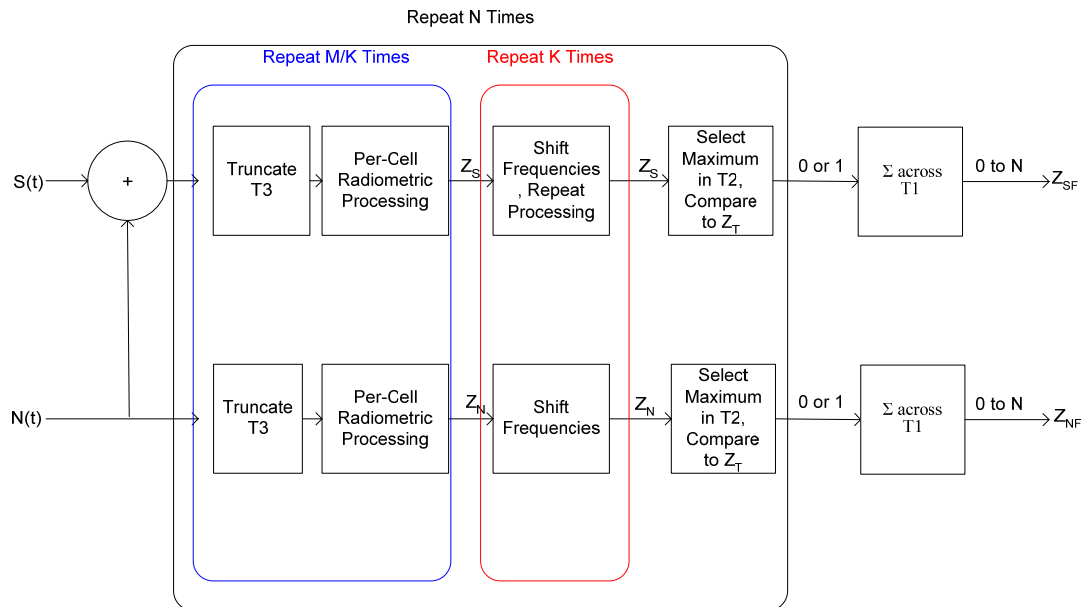


Figure 3.8 Simulated Fast Sweeping Channelized Radiometer Block Diagram

### 3.4 Delay and Multiply Receiver

While not usually used for FH signals, the delay and multiply (D&M) receiver has been the method of choice for Direct-Sequence Spread Spectrum (DSSS) signals. The D&M signal prefilters the signal to a bandwidth of  $W_1$ , delays the signal by an amount (usually the PN chip rate, hence the name chip rate detector), and multiplies the delayed signal with the original signal. This will produce features in the spectrum of the signal, which can be exploited through the use of a very narrow filter. The block diagram (with the width of the second filter given the designation  $W_2$ ) can be seen in Figure 3.9. Figure 3.10 illustrates the feature-detection aspect of the chip rate detector.

The chip rate detector was simulated in the above manner using a 0.5 Hz secondary filter. The width of the filter was arbitrarily chosen to be 0.5 Hz, but it could be any small value (as long as the location of the feature in frequency is known to a high-level of accuracy) since the feature itself is basically an impulse in frequency. Since the FH signal did not have a PN chip rate, the bit rate was used instead. The results for the SOI, which can be seen in Appendix A, were very poor and did not warrant further investigation.

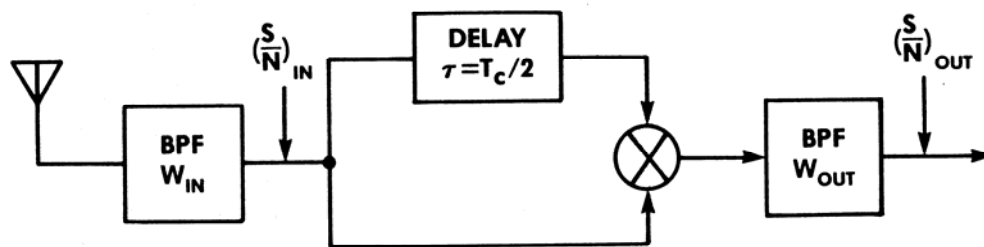


Figure 3.9 Delay and Multiply Receiver Block Diagram [11]

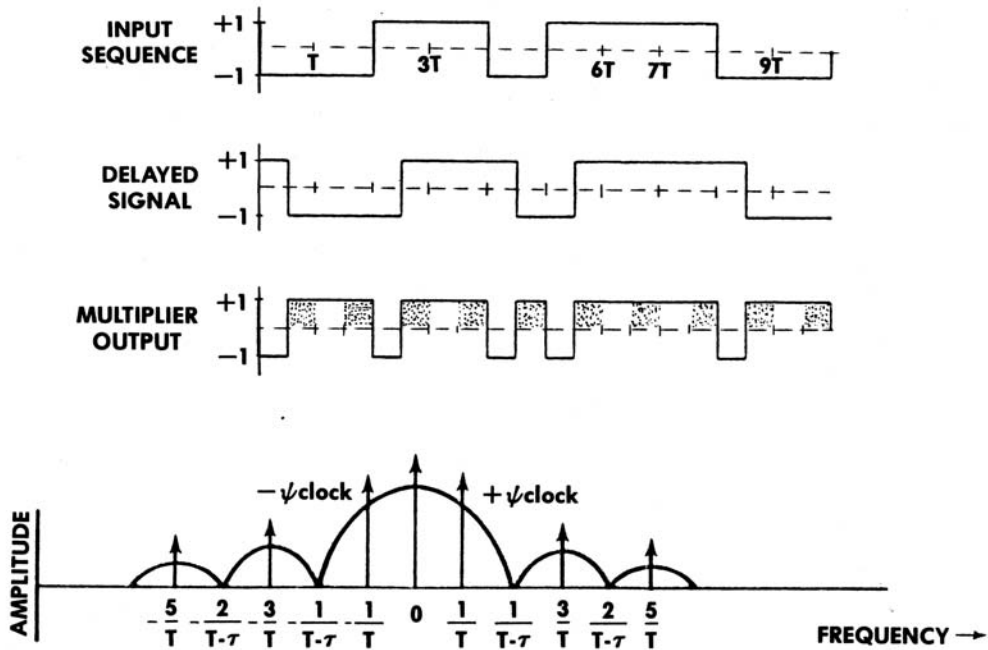


Figure 3.10 Chip Rate Detector Feature Generation [11]

### 3.5 Jamming Transmitters

Two types of jamming transmitters were used for this research: a wideband jammer and a narrowband jammer. In each case it was assumed that only one jammer was transmitting at one time and it was transmitting for the duration of the signal.

**3.5.1 Wideband Jammer.** The wideband jammer was modeled as a variation in the noise floor. The noise floor is fixed at a certain level ( $N_0$ ) from which the signal's power is set to achieve an average SNR. For each trial, the noise level is then varied based on the magnitude of variation (i.e., for a 25% variation the noise floor can increase or decrease by as much as 25% of  $N_0$ ). This noise is then fed into the models pictured above as  $N(t)$ . This process is repeated 10,000 times such that a collection of  $P_D$  and  $P_{FA}$  points can be gathered. These points are then plotted in a  $P_D$  vs.  $P_{FA}$  receiver operating

characteristic (ROC) curve for a single SNR since CFAR thresholding is very difficult with a varying noise floor.

**3.5.2 Narrowband Jammer.** The narrowband jammer emits a BPSK signal at a single fixed frequency of 2 Hz. BPSK was chosen because it is a simple situation with easily-defined bandwidths, energy levels, etc. Ideally the jammer would be able to change frequencies in unison with the communications transmitter, but it assumed here that the jammer does not know the hop pattern, thereby not gaining an advantage by hopping itself. The bandwidth of the jammer is also 2 Hz (the same signal depicted in Figure 2.7), enabling it to disrupt an entire channel at one time.

The energy level of the signal is chosen to achieve a certain SNR with respect to the constant noise floor. The generated interference signal is then combined with  $N(t)$  in the preceding diagrams and then sent to the main processing block. Once again,  $P_D$  vs.  $P_{FA}$  ROC diagrams (as opposed to CFAR plots) are used to represent narrowband jamming data as with the wideband jamming data since CFAR thresholding is very difficult with jamming signals.

### 3.6 Summary

This chapter discussed the techniques used to simulate the signal environment as presented in Chapter 2. The GMSK-FH signal structure (along with assumptions) simulated in this research was presented. Five types of energy detection schemes (wideband radiometer, channelized radiometer, narrowband channelized radiometer, sweeping channelized radiometer, and delay and multiply receiver) were discussed, with the benefits and limitations of each mentioned. The two jamming techniques (wideband and narrowband) were presented along with their methods of simulation. The signal

structure will be tested using the detection schemes mentioned under a variety of conditions in Chapter 4. In addition, the two main detection models (wideband and channelized) will be subjected to the two jamming transmitters.

## **4. Detection Results and Analysis**

### **4.1 Introduction**

This chapter presents a detectability study of the GMSK-FH signal as described in Chapters 2 and 3. Section 4.2 introduces the benchmark for comparison, the wideband radiometer. Section 4.3 discusses how varying the signal parameters affects signal detectability. Section 4.4 describes the effects of changing the classic channelized radiometer scheme to include the narrow-bandwidth channelized radiometer and the sweeping channelized radiometer. Finally, Section 4.5 describes the effects of both broadband and narrowband jamming.

### **4.2 Wideband Baseline for Comparison**

As discussed in Chapter 2, it is the goal of the intercepting party to gain as much information about the signal as possible under the given conditions. To do this, it must use the most sophisticated and flexible intercept receiver available. In this case, that would be the channelized radiometer. The interceptor, due to environmental factors and limitations, may find the wideband radiometer to provide superior detection performance under certain conditions. The transmitter, of course, would like to force the interceptor to use the wideband radiometer as the detection scheme of choice as much as possible.

The baseline for all comparative analysis in this report is the theoretical wideband radiometer as presented in Chapter 2. The analytical version is chosen over the simulated version to achieve a higher level of accuracy. However, when the situation cannot be analytically derived (as is the case with the sweeping channelized radiometer), simulated results are used.



Figure 4.1 is a plot of wideband radiometer  $P_D$  versus SNR for a  $P_{FA}$  of 0.01, a signal duration of 96 bits ( $T_I$ ), and a bandwidth ( $W_I$ ) of 30 Hz. For all plots given in this chapter, SNR refers to the ratio of the average signal power to the average noise power.

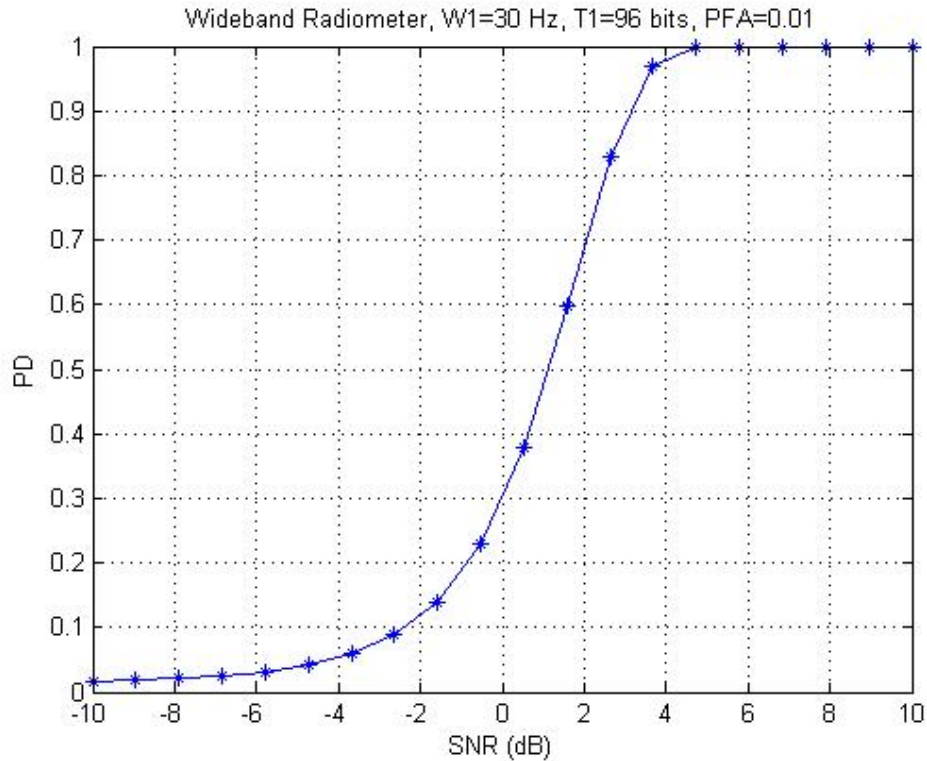


Figure 4.1 Wideband Radiometer,  $T_I=96$  bits,  $W_I=30$  Hz, and  $P_{FA}=0.01$

This plot shows that for the given  $P_{FA}$ , as the desired  $P_D$  increases, the intercept receiver requires a higher SNR (which translates to a shorter intercept range as outlines in Chapter 2). Thus, the interceptor would prefer a situation in which the detection curve for the channelized radiometer (or other advanced detection scheme) will be to the left of the wideband radiometer.

### 4.3 Effects of Changing Signal Parameters on Detection Performance

Chapter 3 outlined the signal parameters used for this research. The three key variable parameters are signal duration, hop rate, and jitter. This section examines the effects of changing these parameters one at a time.

**4.3.1 Altering Signal Duration.** The default signal duration is 96 bits, which in this research is the longest duration the signal can exist. Figure 4.2 is a plot of the signal with a duration of 96 bits undergoing both interception methods (the signal is assumed to have the other default characteristics as presented in Chapter 3).

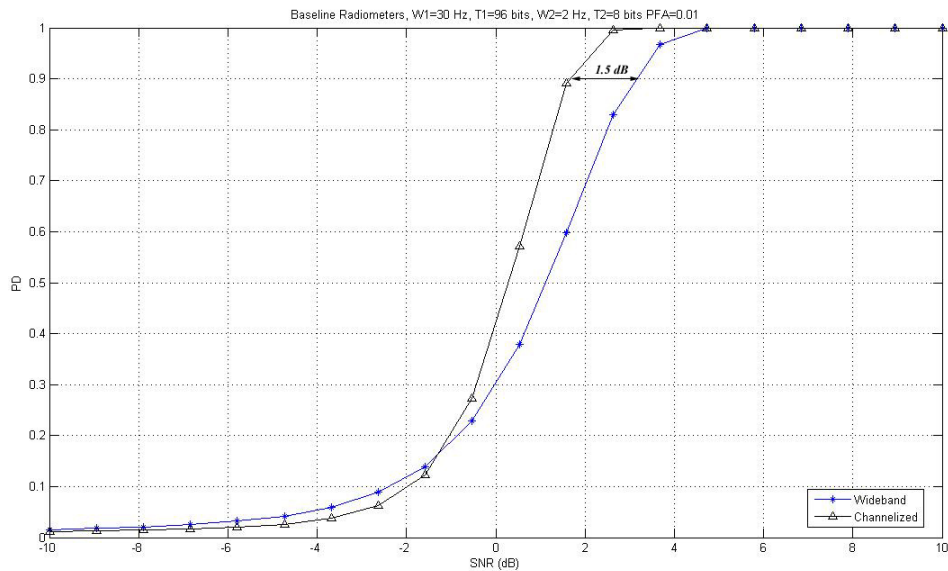


Figure 4.2 Wideband vs Channelized Radiometer,  $T_I=96$  bits

This plot shows that the channelized radiometer curve is steeper than the wideband radiometer curve, meaning that it is more sensitive to changes in SNR. Using the  $Q_{INT}$  as defined in Chapter 2 (with a  $P_{FA}=0.01$  and  $P_D=0.9$  for all cases throughout this Chapter), this scenario (which will be the baseline for all future tests) has a  $Q_{INT}$  of 1.5 dB. Thus, if a new scenario produces a higher  $Q_{INT}$  (meaning the wideband radiometer has a relatively greater increase in its  $SNR_{req}$  than the channelized radiometer),

the channelized radiometer will be at an advantage. If not, the wideband radiometer gains a relative advantage from the change in parameters, even though its overall ability to detect the signal may decrease.

Figure 4.3 shows the effects of shortening the signal to its minimum duration of 40 bits.

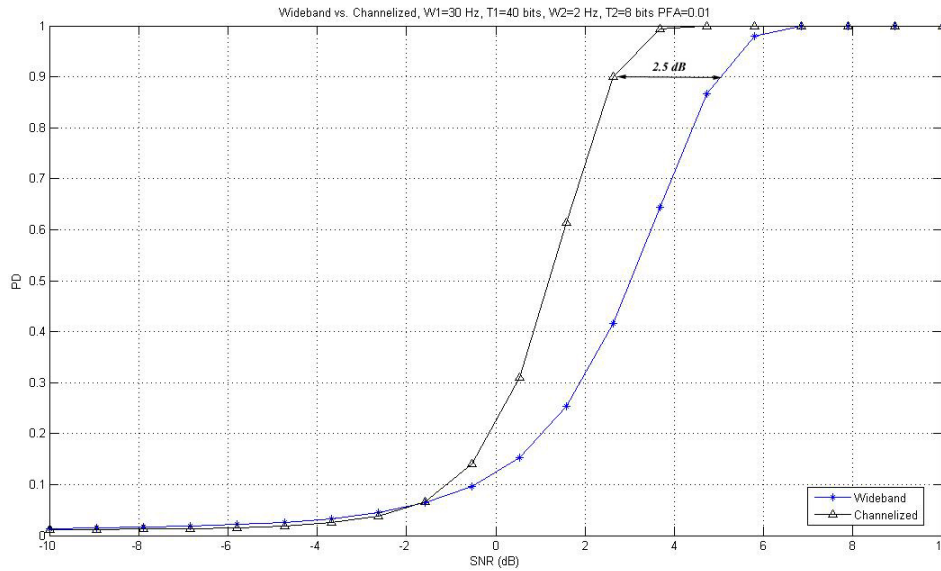


Figure 4.3 Wideband vs. Channelized Radiometer,  $T_I=40$

This figure shows that the  $Q_{INT}$  for the reduction in signal duration is 2.5 dB, which is 1.0 dB to the advantage of the channelized radiometer. Hence, a decrease in  $T_I$  will lead to a *relative* advantage for the channelized radiometer. However, it must be noted that the  $SNR_{req}$  for both receivers increased with the decrease in signal duration, indicating that both receivers would have to move in closer to the communication transmitter in order to maintain performance goals. As an illustration, the increase in  $SNR_{req}$  of 0.9 dB will require the channelized radiometer to reduce its range to the communications transmitter by approximately 10% per equation (2.5). Thus, the interceptor is at an overall disadvantage.

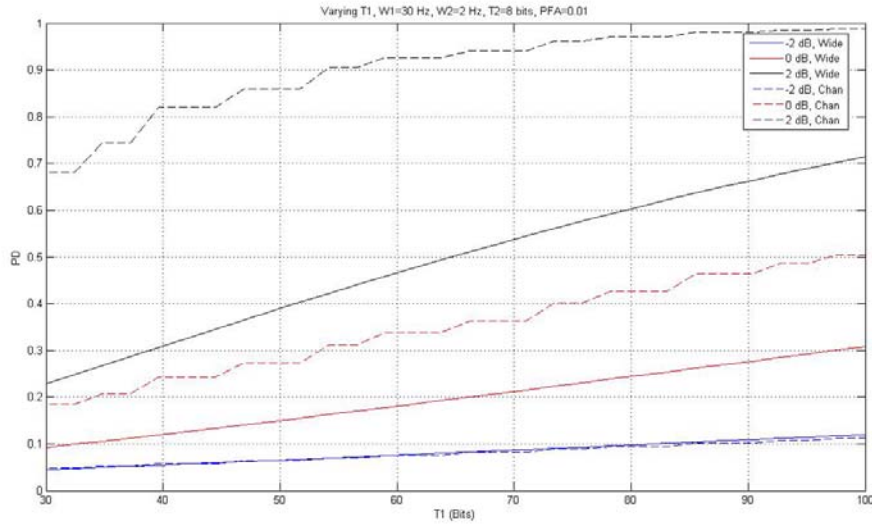


Figure 4.4 Varying  $T_1$  from 30 bits to 100 bits

Figure 4.4 is a plot of  $P_D$  vs.  $T_1$  for three sample SNRs at the  $P_{FA}$  of 0.01. This shows that both the channelized and wideband radiometers experience performance improvements with an increase of  $T_1$ . The rates of improvement for the given SNRs are roughly the same, which indicates changing  $T_1$  does not have a strong effect on relative performance, unlike the upcoming cases where the wideband radiometer demonstrates a horizontal graph.

**4.3.2 Altering Hop Rate.** The hop rate of the signal (the number of hops/second) determines the channelized radiometer's  $T_2$  parameter (as stated in the assumptions, the channelized radiometer is assumed to know this information ahead of time). The default hop rate is 1/8, or inversely 8 bits per hop. Thus, the default  $T_2$  for the channelized radiometer is also 8 bits. It becomes clear that changing the hop rate should have no effect on the performance of the wideband radiometer since it is only concerned with the total amount of energy in the signal, not the per-hop amount of energy.

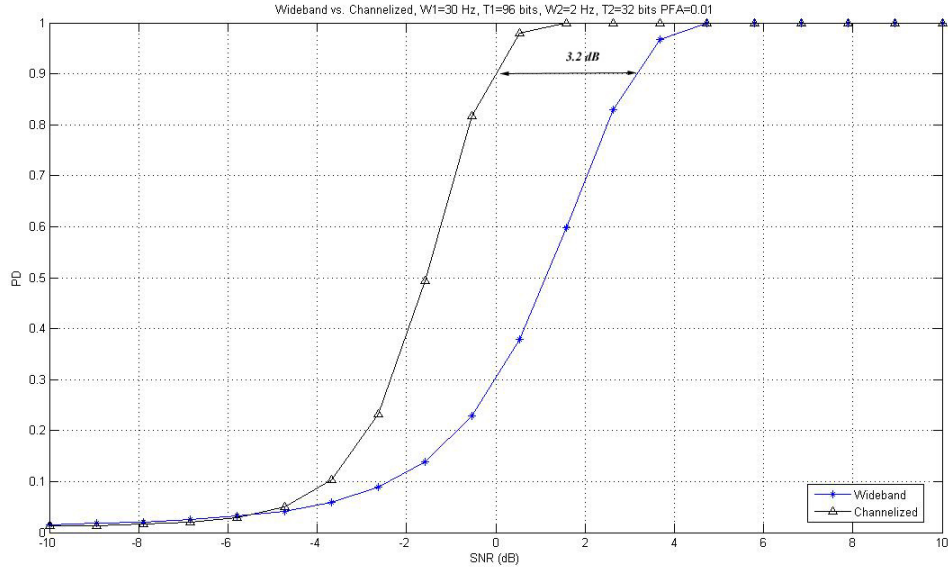


Figure 4.5 Wideband vs. Channelized Radiometer,  $T_2=32$  bits

Figure 4.5 demonstrates the effect of reducing the hop rate from 1/8 to 1/32. The  $Q_{INT}$  for this case becomes 3.2 dB, which corresponds to a relative advantage of 1.7 dB for the channelized radiometer. The wideband radiometer was not affected at all because it has nothing to do with the  $T_2$  parameter, as shown in Figure 4.6.

Figure 4.6 is a plot of the two detection schemes for the same SNR values in Figure 4.4 undergoing a change in hop rate (from 1/20 hops/sec to 1 hop/sec). As expected, the wideband radiometer does not experience a change in performance when the hop rate is altered. However, the channelized radiometer experiences a sharp decrease and then asymptotically approaches a  $P_D$  of 0, obtained by forcing  $T_2$  to 0 (and  $N \rightarrow \infty$  as a result) in the channelized radiometer equations in Chapter 2. If the communication transmitter knows the intercepting party is using a channelized radiometer, it should make an effort to increase its hop rate such that the channelized radiometer's performance will be significantly degraded. There are some artifacts in the plot at very low hop rates. This is due to the fact that at these higher  $T_2$  values the

channelized radiometer must make a decision based on a very low number of hops (part of the double thresholding complications), making the results appear to be coarse at these values.

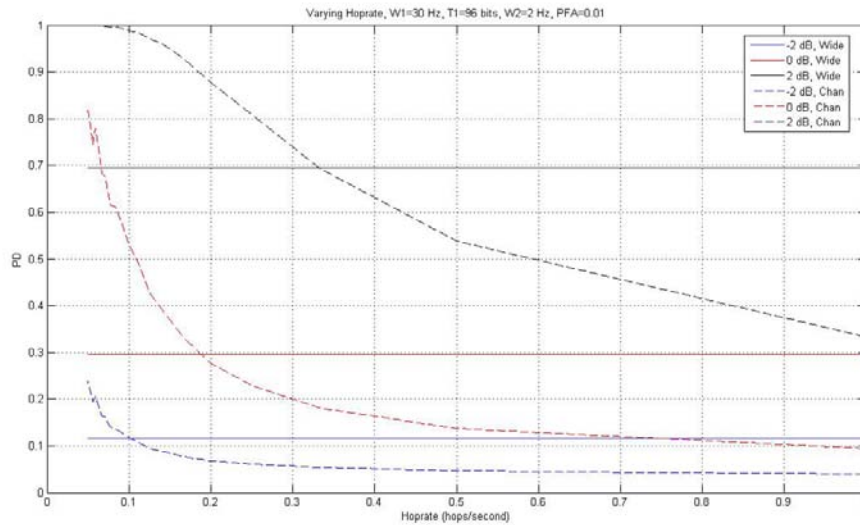


Figure 4.6 Varying Hop Rate (1/20 hops/sec to 1 hop/sec)

**4.3.3 Altering Jitter.** As mentioned in Chapter 3, jitter is the signal’s ability to change its position in time, a form of time-hopping. For this research, since the energy detection methods presented are not concerned with position of signal (merely total energy in a given “cell”), jitter is defined as the percentage reduction in signal duration per hop. For instance, if  $T_2=8$  seconds (hop rate of 1/8) and the signal is said to have a 10% jitter, the signal will then occupy 90% of  $T_2$ , or a per-hop signal duration of 7.2 seconds. The signal will essentially be turned off for the last 0.8 seconds of the hop before it hops again. However, the channelized radiometer will still be set at a  $T_2$  of 8 seconds, because the channelized radiometer in this case does NOT have *a priori* knowledge of jitter. Therefore, the receiver must assume the no-jitter scenario to be all-inclusive. As a result, introducing jitter will degrade the performance of the channelized

radiometer because there will be less signal compared to the same amount of noise. The wideband radiometer will also experience an effect because it will have to cope with less signal energy in  $T_I$ .

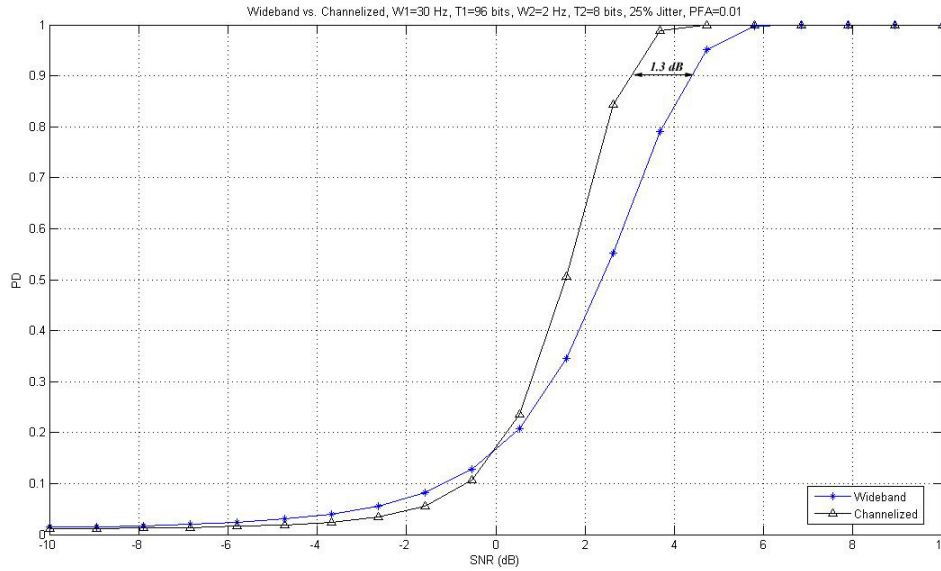


Figure 4.7 Channelized vs. Wideband Radiometer, Jitter=25%

Figure 4.7 shows the effects of adding a jitter of 25% to the signal. The  $Q_{INT}$  for this case becomes 1.3 dB, which yields a 0.2 dB relative disadvantage for the channelized radiometer. Both receiver models experienced degradation. This is due to the fact that there is simply less signal in the  $W_I \times T_I$  signal space while the amount of noise remains the same.

The effects of varying jitter are presented in Figure 4.8. The plot shows a decrease in performance for both models as the amount of jitter increases, which is in accordance with predictions. The 0 dB pair clearly shows a crossover point at which the wideband radiometer outperforms the channelized radiometer. Thus, the transmitter would like to incorporate jitter into its communication system. However, the

communication receiver would have to deal with less signal energy as a result as well as synchronization issues, but those concerns are beyond the scope of this research.

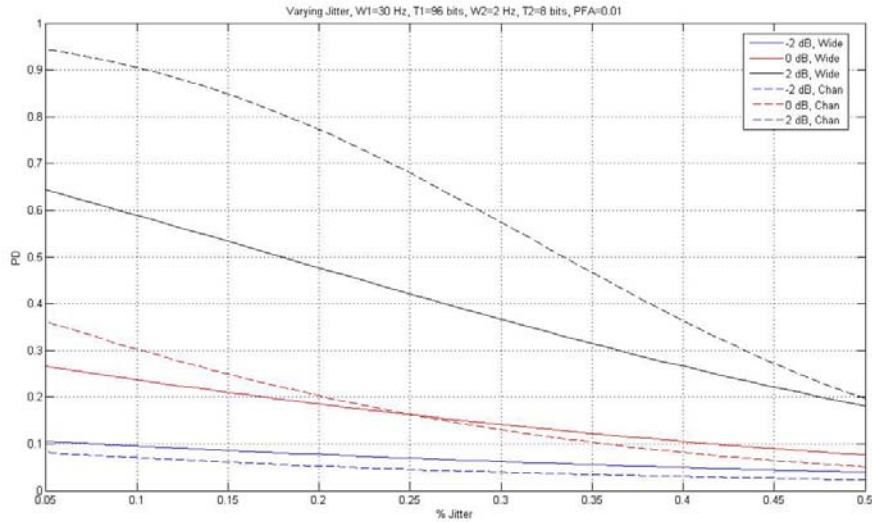


Figure 4.8 Varying Jitter 5% to 50 %

#### 4.4 Changes to the Standard Channelized Radiometer Model

The channelized radiometer as presented thus far has been developed with the assumption that the entire  $W_I$  frequency spectrum is covered and the interceptor hardware is able to process 15 channels concurrently. When these assumptions are relaxed, the performance of the channelized radiometer changes accordingly. Two situations will be examined: 1) the channelized radiometer is able to “pinpoint” the signal hop frequencies and 2) the intercept receiver is limited to 5 channels instead of the necessary 15.

**4.4.1 Narrow-Bandwidth Channelized Radiometer.** The standard channelized radiometer consists of 15 channels with a bandwidth of 2 Hz each to cover the entire 30 Hz spectrum. Each channel is adjacent to the next without any gaps in between. Since the GMSK waveform is narrowband, with a 3 dB bandwidth of 0.3 Hz in this case, there is no need to have a 2 Hz bandpass filter for each channel if the exact hop frequency is



known. By reducing the bandwidth of each channel such that gaps appear between adjacent channels, less noise enters the filter and a performance improvement can be expected.

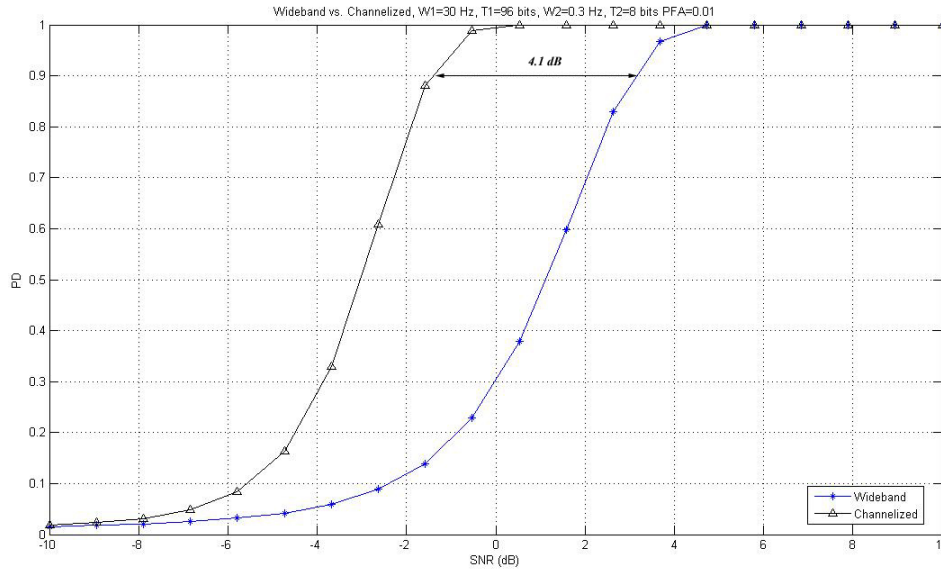


Figure 4.9 Channelized vs. Wideband, Narrow Bandwidth

Figure 4.9 illustrates the effect of reducing the bandwidth of the channelized radiometer’s channels. It is clear that the narrow bandwidth has a dramatic improvement on the channelized radiometer’s performance. The  $Q_{INT}$  is 4.1 dB, which translates to a relative advantage of 2.6 dB for the channelized radiometer. The wideband radiometer is not affected, much like the changing hop rate case. This is due to the fact that for each cell examined by the channelized radiometer, there is slightly less signal but significantly less noise (since the noise PSD is flat while the signal PSD has a peak at the hop frequency, as was shown in Figure 2.7).

This narrow bandwidth receiver would be very difficult to implement because of the frequency drift of the transmitted signal. If the bandwidth of the channel is to be reduced by a substantial amount, it must be able to very accurately know the location of

the hopped frequency. The results obtained above assumed perfect knowledge of the transmitted frequency. However, with such a narrow filter the price for drifting away from the actual frequency increases. This becomes especially problematic in high-speed airborne communication platforms because there tends to be a Doppler shift in the signal's frequency. As a result, it becomes even more difficult to determine the exact location of the hopped frequency. In conclusion, decreasing the bandwidth of the channel would be beneficial, as long as the external factors are kept in mind.

**4.4.2 Sweeping Channelized Radiometer.** As Chapter 3 indicated, it is not always possible to have as many channels in the channelized radiometer as is necessary to cover the entire spectrum. The most common method to deal with this issue is the introduction of the sweeping channelized radiometer. The sweeping radiometer can operate in one of two methods, slow-sweep and fast-sweep, as discussed in Chapter 3.

In the slow-sweeping channelized radiometer, it is nearly impossible to detect the signal during each and every hop because only a percentage of the available bandwidth is covered per hop. Thus, there is a certain miss probability  $P_M=1-P_D$ , where a signal is present but not declared. This phenomenon is demonstrated by the slow-sweeping intercept receiver's inability to achieve a  $P_D$  greater than 0.3, regardless of input SNR in Figure 4.10. The slow-sweep radiometer in this case has five 2 Hz channels, enabling it to cover 1/3 of the available spectrum per hop. This can be derived theoretically by using the same channelized radiometer equations in Chapter 2 with some alterations of  $p_0$  and  $p_1$ .

If there are  $K$  hops per one complete sweep, the per-hop probability of intercept ( $POI$ ) is  $1/K$ . Likewise, if there are  $M/K$  radiometer outputs per hop, this becomes the effective number of outputs, or  $N_{eff}$ . Thus, (2.18) becomes

$$p_0 = 1 - (1 - Q_F)^{N_{eff}} \quad (4.1)$$

and (2.20) becomes

$$p_1 = 1 - (1 - Q_D)(1 - Q_F)^{N_{eff}-1} + (1 - POI)p_0 \quad (4.2)$$

The summation in (4.2) is possible because the two events (the probability of detection and the probability of a false alarm resulting from a missed detection) can be assumed to be independent and mutually exclusive [10].

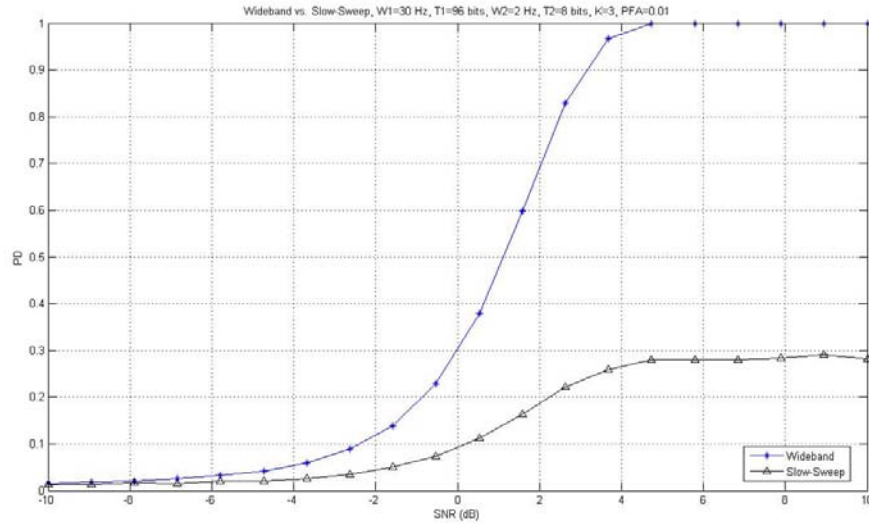


Figure 4.10 Wideband Radiometer vs. Slow-Sweep Channelized Radiometer

The fast-sweep radiometer was also tested. With the number of channels still set at 5, the fast-sweep is able to cover the entire spectrum within one hop interval, but can only do so by integrated for  $1/3$  of the time of the standard channelized radiometer. With less time to integrate, less of the signal can be observed at one time (similar to increasing the hop rate). The net effect is a degradation in performance as shown in Figure 4.11.

The  $Q_{INT}$  becomes -3.9 dB, which is -5.4 dB from the baseline case. The interceptor clearly suffers from using sweeping channelized radiometers.

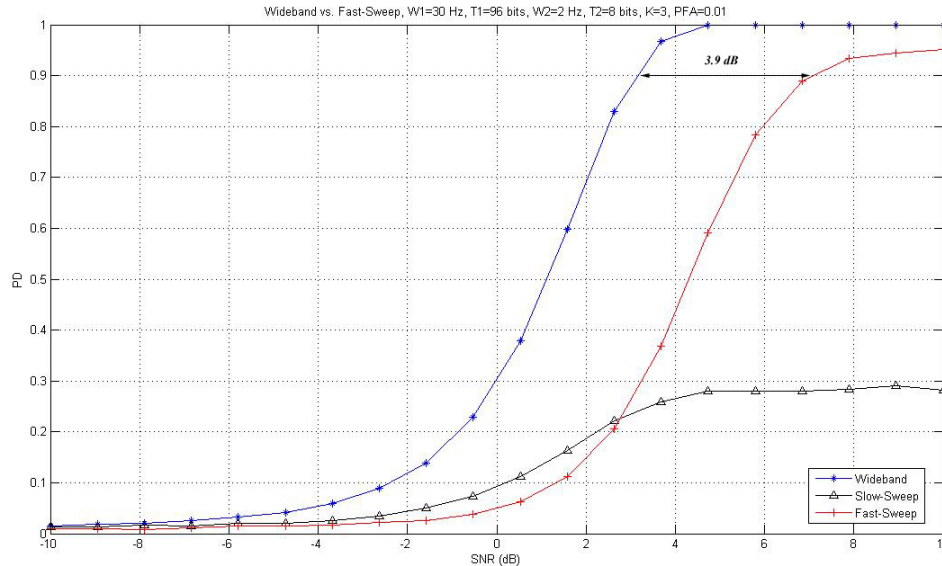


Figure 4.11 Wideband vs. Sweeping Channelized Radiometers

## 4.5 Jamming

The last two sections deal exclusively with the signal of interest and the detection models. In this section, jamming is introduced into the scenario. Two types of jamming are tested: broadband jamming and narrowband jamming. Each jamming scenario is used in conjunction with both standard non-cooperative detection models.

**4.5.1 Wideband Jamming.** One possible jamming method is wideband jamming. The jamming transmitter emits a very wide bandwidth signal in the attempt to disrupt communication signals that have very wide bandwidths. Since communication techniques such as Ultrawideband are becoming more popular, it is becoming more difficult for narrowband jammers to operate effectively.

For the purposes of this research, the wideband jammer has been modeled as a change in the noise floor level. The noise floor still maintains a constant average power,

but it varies within a fixed bound that is a percentage of the average thermal noise power. Three bounds have been tested: 10%, 25%, and 50%. The results for this test are also presented differently. The varying noise floor makes CFAR processing very difficult, so instead of the standard  $P_D$  vs. SNR plot, a  $P_D$  vs.  $P_{FA}$  plot, commonly called a Receiver Operating Characteristic (ROC) Curve, is used instead. The further the curve rises to the upper left, the better the performance of the detection receiver since a larger  $P_D$  is achieved with the same  $P_{FA}$ . A curve that looks like a straight line rising at  $45^\circ$  ( $P_D=P_{FA}$ ) is indicative of a very poor detection receiver as it is essentially correct 50% of the time, which is no better than a random coin toss.

Figure 4.12 is a plot of the Wideband Radiometer under the influence of a wideband jammer. The constant-noise SNR of the signal is 0 dB and three noise variations are used: 0%, 25%, and 50%. The performance of the wideband radiometer degrades significantly when the noise floor varies. It is interesting to note that the fact the noise floor is actually lower half the time does not counteract the raising of the noise floor. There is not much difference between 25% and 50% variations for the original value of 0 dB.

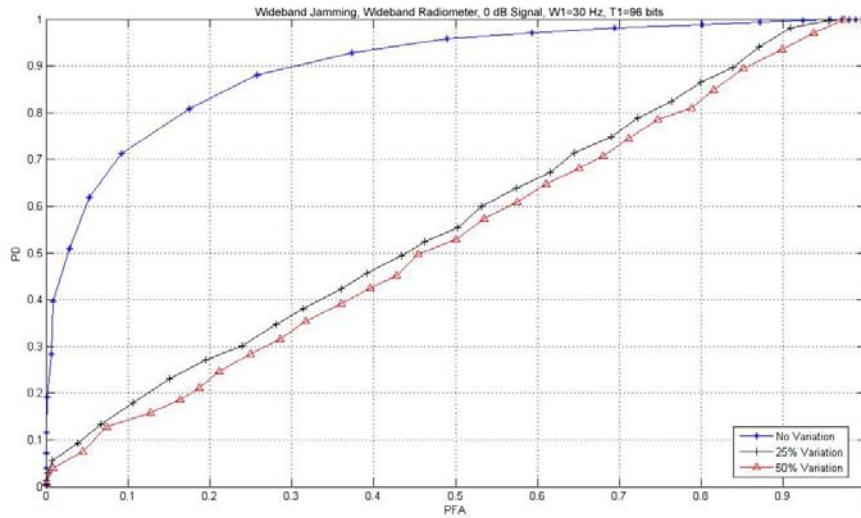


Figure 4.12 Wideband Radiometer with Wideband Jamming

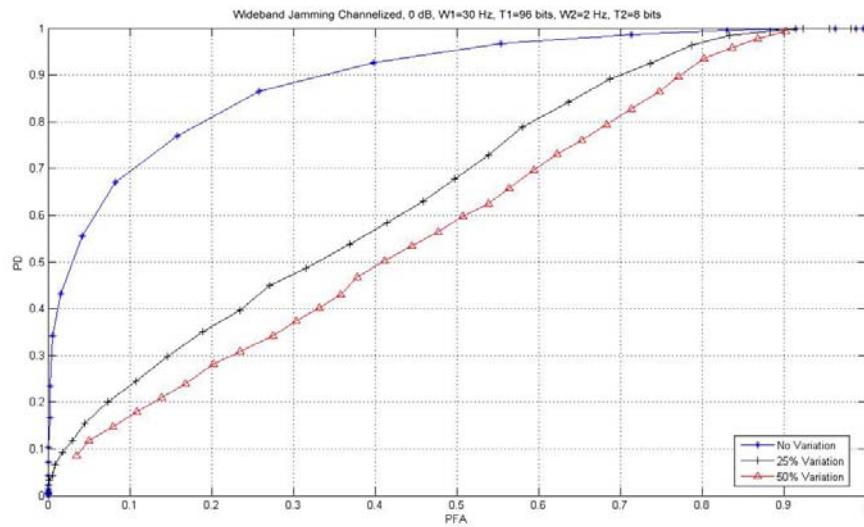


Figure 4.13 Channelized Radiometer with Wideband Jamming

Figure 4.13 examines the effects of a wideband jammer on the channelized radiometer. The effects are not quite as pronounced as they were with the wideband radiometer, but they are still significant. Figure 4.14 is a plot of both models under the influence of wideband jamming. While the wideband and channelized radiometers have roughly the same performance characteristics at an SNR of 0 dB without jamming, the

presence of a wideband jammer actually favors the channelized radiometer, since it has a higher  $P_D$  for a given SNR and  $P_{FA}$ . This is due to the channelized radiometer using a smaller percentage of noise for each integration cell. Since the variation in noise is constant across all frequencies, the variations will not affect one channel more than another, which is not the case with narrowband jamming.

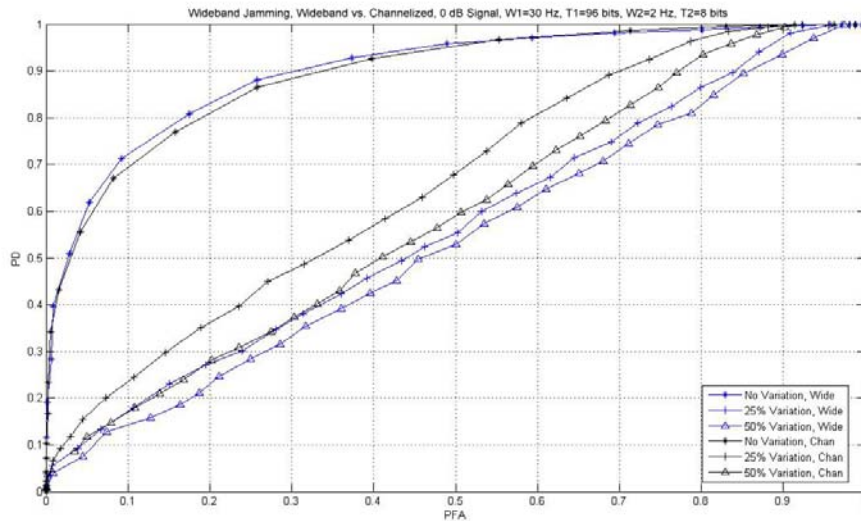


Figure 4.14 Wideband vs. Channelized Radiometer with Wideband Jamming

**4.5.2 Narrowband Jamming.** The other method of jamming explored is narrowband jamming. In narrowband (or single-tone) jamming the interfering transmitter uses a significantly smaller bandwidth but is therefore able to transmit at a higher power. The simulations performed for this research assume the single-tone jammer will occupy the equivalent bandwidth of one channel. Ideally the jamming transmitter would know the hop pattern of the FH transmitter and therefore be able to completely disrupt the signal. In this case, it is assumed that the jamming transmitter does not know this, so it transmits continuously at one carrier frequency.

The jammer was simulated using several different power levels expressed as jamming to noise ratio that is equal to the average power of the jamming signal divided by the average thermal noise power. The results for the wideband radiometer are shown in Figure 4.15, using the  $P_D$  vs.  $P_{FA}$  representation once again.

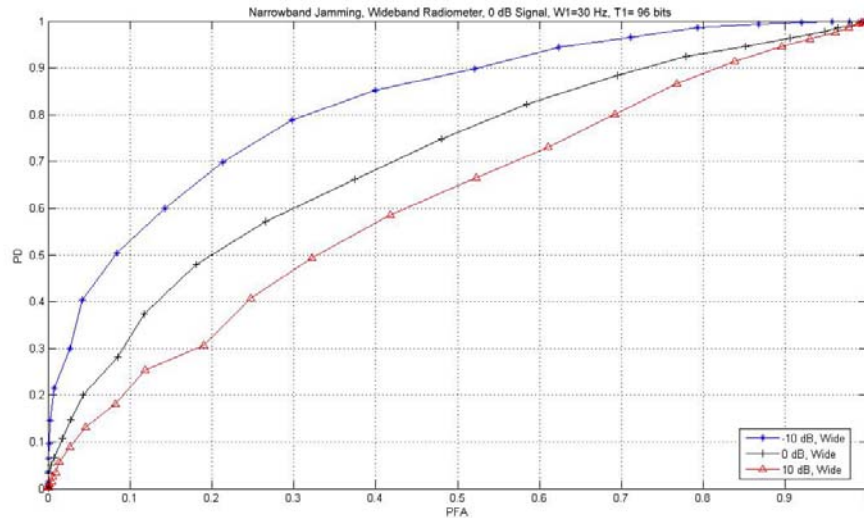


Figure 4.15 Wideband Radiometer with Narrowband Jamming

There is a degradation in performance with the introduction of the jammer, with the  $P_D$  dropping proportionally to the power of the narrowband jammer. The results for the channelized radiometer are shown in Figure 4.16. The dual plot in Figure 4.17 illustrates the effect of the narrowband jammer on the channelized radiometer. Even a -10 dB jamming signal renders the channelized radiometer almost completely useless with the  $P_{FA}=P_D$  line becoming evident. While the channelized and wideband radiometers have virtually the same performance with a 0 dB signal as seen in Figure 4.14, the results are very different when narrowband jamming is introduced. Thus, if the intercept receiver was working in tandem with a jamming transmitter, the intercept receiver would be wise to suggest a jamming approach that did not use narrowband jamming over one of



the channelized radiometer's channels, or else the preferred method of interception (the channelized radiometer) would not be useful at all. Similarly, if the communication party were using jammers, they would be well suited to use a narrowband jammer.

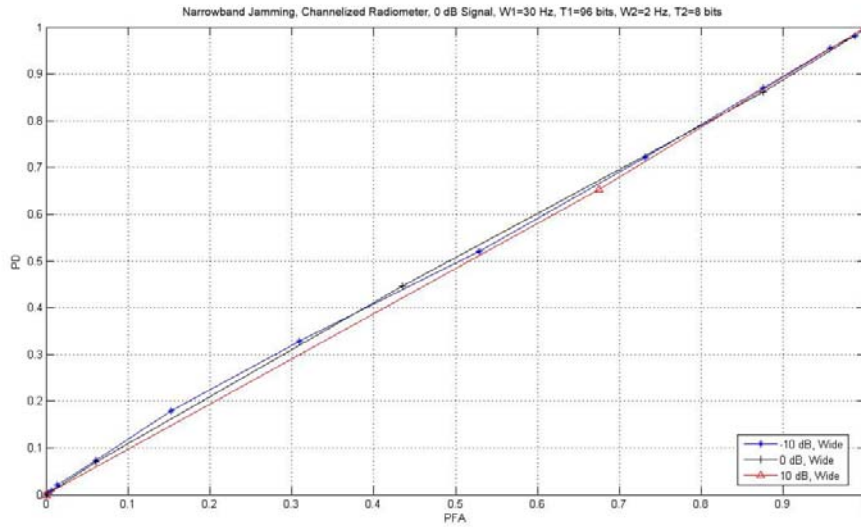


Figure 4.16 Channelized Radiometer with Narrowband Jamming

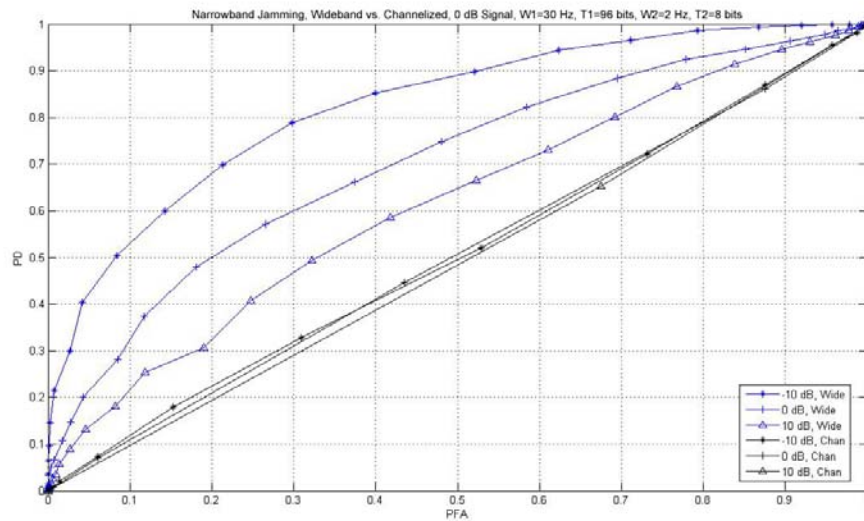


Figure 4.17 Wideband vs. Channelized Radiometer with Narrowband Jamming

It is also interesting to note that the narrowband jammer in this case does not require a frequency hop capability to be effective: flooding one channel is enough to

severely disrupt the receiver. The channelized receiver may want to incorporate an algorithm that can reject such interfering signals.

#### 4.6 Summary

The wideband radiometer was presented as a baseline intercept receiver model for comparison. With the desire to use the channelized radiometer over the wideband radiometer in mind, the receiver models developed in Chapters 2 and 3 were applied to the signal of interest. The signal's parameters were modified and the changes in receiver performance were noted. The channelized radiometer model then underwent changes and the results on detection performance were also analyzed. The following table summarizes the results.

Table 4.1 Summary of Test Results

Test	Plot	Results ( $\Delta Q_{INT}$ or $\Delta P_D$ )
Shortening $T_1$ from 96 to 40	$P_D$ vs. SNR	Channelized improved by 1 dB (also degraded 0.9 dB overall, decreasing range by 10%).
Varying $T_1$	$P_D$ vs. $T_1$	Channelized and Wideband both steadily improve as $T_1$ increases. Wideband at a slightly higher rate.
Reducing Hop rate from 1/8 to 1/32	$P_D$ vs. SNR	Channelized improved by 1.7 dB, increasing range by 22%.
Varying Hop rate	$P_D$ vs. Hop rate	Wideband is unaffected by changes in hop rate (not dependent upon $T_2$ ). Increasing Hop rate decreases performance of Channelized.
Introducing 25% Jitter	$P_D$ vs. SNR	Channelized degraded by 0.2 dB (also degraded 2.6 dB overall, decreasing range by 26%)
Varying Jitter	$P_D$ vs. Jitter	Both Wideband and Channelized degrade with increasing jitter. Channelized degraded to a higher degree.
Reducing Channelized $W_2$ from 2 to 0.3	$P_D$ vs. SNR	Channelized improved by 2.6 dB, increasing range by 35%

Test	Plot	Results ( $\Delta Q_{INT}$ or $\Delta P_D$ )
Slow Sweep and Fast Sweep Channelized, K=3	$P_D$ vs. SNR	Slow Sweep asymptotically approaches $P_D=0.3$ , Fast Sweep degrades channelized by 5.4 dB, decreasing range by 46%
Wideband Jamming (50% variation in noise floor)	$P_D$ vs. $P_{FA}$	Variation of 50% $\rightarrow$ Channelized relatively 0.5 $P_D$ better than baseline at $P_{FA}=0.1$
Narrowband Jamming for Wideband and Channelized. Signal Power remains constant.	$P_D$ vs. $P_{FA}$	10 dB Jamming $\rightarrow$ Channelized relatively 0.1 $P_D$ worse than baseline at $P_{FA}=0.1$ . Both significantly degraded (coin-toss case).

## 5. Conclusions

### 5.1 Summary

This thesis was dedicated to analyzing the tactical communication scenario and determining the party (communicator vs. interceptor) that would benefit most from changes in individual parameters within the environment. Two types of detection methods were examined in detail: the wideband radiometer and the channelized radiometer. A delay and multiply intercept receiver was also considered, but proved to have such poor performance that it was immediately discounted as a viable candidate receiver to undergo the entire battery of tests. The communication signal had the same basic structure, with modifications added to test the abilities of the intercept receivers.

The receiver models were used to non-cooperatively detect the signal of interest in a variety of situations. Each modification to the receiver, signal, or environment occurred one at a time in order to examine the effects of the single parameter that was altered. The following alterations were made:

Table 5.1 Tested Parameters

<b>Signal Parameters</b>	<b>Receiver Parameters</b>	<b>Environmental Parameters</b>
Signal Duration	Channelized Receiver Channel Bandwidth	Wideband Jamming
Hop Rate of Signal	Number of Channelized Receiver Channels	Narrowband Jamming
Presence of Jitter		

For each test, plots were generated comparing the two receiver models under test depicting probability of false alarm ( $P_{FA}$ ), probability of detection ( $P_D$ ), and signal to noise ratio (SNR). An interception quality factor  $Q_{INT}$ , was developed to determine the best receiver design for the particular scenario. If the channelized radiometer reduced its

$SNR_{req}$  relative to the wideband radiometer, the  $Q_{INT}$  increased and the channelized radiometer gained a relative advantage for the case in question. In the jamming cases where CFAR processing is much more challenging, the winning receiver had the highest  $P_D$  for a given  $P_{FA}$  and SNR. The intercepting party gains a definite advantage by using the channelized radiometer because of its greater potential for exploiting the signal versus the wideband radiometer. Thus, the intercepting party desires situations that will increase  $Q_{INT}$ . However, the fact that  $Q_{INT}$  increases does not automatically indicate a “victory” for the intercepting party: if  $SNR_{req}$  for both receiver models increases, the communicating party forces the intercept receiver to move closer to the transmitter regardless of intercept receiver, which is what the communicating party desires.

## 5.2 Conclusions

**5.2.1 Scenarios Beneficial to the Communicating Party.** The communication party gained a situational advantage whenever the  $SNR_{req}$  for the intercept receivers increased. This occurred when intentional jitter was introduced, jamming was present, signal duration  $T_1$  and hop duration  $T_2$  decreased, and a sweeping channelized radiometer was used. The amount of benefit gained will depend upon the receiver model used by the intercepting party. When  $Q_{INT}$  increased as  $SNR_{req}$  increased (as was the case with a decrease in  $T_1$ ) the wideband radiometer experienced a greater degradation in performance relative to the channelized radiometer. Since the channelized radiometer poses the greater threat to the communicator, the communicator would prefer to incur a degradation that affects the channelized radiometer to a greater degree than the wideband radiometer (i.e.,  $Q_{INT}$  decreases). This is exactly the case with increased jitter and the use of a narrowband jammer, which would be the preferred methods to increase  $SNR_{req}$ . In

truth, introducing such means of disruption as intentional jitter, jamming, and high hop rates will undoubtedly call for increased receiver complexity. In a similar manner, the channelized radiometer used here was unable to distinguish/eliminate narrowband jamming signals. If it did possess that capability, the communication receiver would likely suffer more in jamming situations than the interceptor.

**5.2.2 Scenarios Beneficial to the Intercepting Party.** The interception party benefited whenever  $SNR_{req}$  decreased, allowing the distance from the communication transmitter to increase for a given set of performance parameters. Since the channelized radiometer has a much greater potential for signal exploitation through advanced processing techniques, situations that both reduce  $SNR_{req}$  and increase  $Q_{INT}$  are highly desired. This occurred with a decrease in receiver channel bandwidth  $W_2$  as well as a reduction in hop rate. Since signal parameters such as hop rate, signal duration, and intentional jitter are beyond the control of the interceptor, the interceptor should focus on accurately determine the channel frequencies (necessary to reduce  $W_2$ ) and implementing jam-resistant measures. If the channelized radiometer were to implement measures to mitigate the effects of narrowband jamming, the intercepting party could then employ jamming techniques to disrupt the communication receiver without suffering degradation itself. As the sweeping channelized radiometer results demonstrated, the intercepting party will suffer greatly if the channelized radiometer does not have the resources to observe the  $W_1 \times T_2$  signal space in its entirety.

### **5.3 Recommendations for Future Research**

**5.3.1 Introduce Doppler Shift.** This research made many simplifying assumption in regards to the background environment (stationary AWGN, etc.). The

most important and potentially severe restriction was placed on the likely introduction of Doppler shift. Since the modeled waveform is to be used in airborne platforms moving at high rates of speed, there will undoubtedly be some frequency shifting as a result of the Doppler effect. This has the potential to disrupt both communication and interception links, but it is especially troublesome with the channelized radiometer, with relatively narrow bandpass filters that leave very little room for error. The reduction in  $W_2$  was shown to be highly beneficial to the channelized radiometer, but it cannot be done without very precise knowledge of the hop frequencies, which may be very difficult when severe Doppler shift occurs. Methods to mitigate the Doppler effect through the accurate estimation of hop frequencies should be explored.

**5.3.2 Recognize Multiple Signals in the Environment.** As stated earlier one of the benefits of the channelized radiometer is its potential to differentiate between different signals in the environment. This research used a channelized radiometer that had no discriminatory abilities. As such, it was severely degraded by narrowband jamming. If the jamming signal were to be removed (perhaps with a tunable notch filter), the degradation of intercept performance would be drastically reduced and the jamming signal becomes a greater concern for the communication link. Many methods for eliminating unwanted signal energy are employed in radar systems, some of which may have applicability in communication systems.

**5.3.3 Use Actual Signal Data.** This research used an approximated waveform that was a simplified version of what is used in airborne datalinks. While the simulated parameters were close to the real parameters, the actual signal may contain timing and/or header information not contained in the simulated signal that can potentially contain

features beneficial to radiometric detection. Likewise, the actual signal may have hidden LPI characteristics not captured in the given parameters. Finally, the simulation of an actual signal could yield more definitive, absolute performance results as opposed to the relativistic results reported in this research.

**5.3.4 Use Multiple Antennas.** As shown in Chapter 2, the antenna effects were disregarded for this research. However, antennas can be used by an interceptor to its advantage. An interceptor with multiple antennas can use spatial diversity to differentiate and exploit various signals of interest. An interesting method was developed in [12] that demonstrated how a three-dimensional interception model can be constructed using spatially-diverse antennas that effectively eliminate noise from the signal space. This technique obviously requires significantly more processing than the two dimensional models used in this research, but the benefits could prove to be more than compensatory.



## Appendix A. Delay and Multiply Receiver Results

The results presented in this section were simulated using the delay and multiply (D&M) receiver model as explained in Chapter 3. For all tests the delay was one half of the bit rate, making it in essence a chip rate detector. The narrowband filter had a bandwidth of 0.5 Hz. Unlike the results presented in Chapter 4, the simulations performed here used a  $P_{FA}$  of 0.1 to reduce the amount of processing time. However, the relative effects are still the same.

### A.1 Baseline Signal Parameters

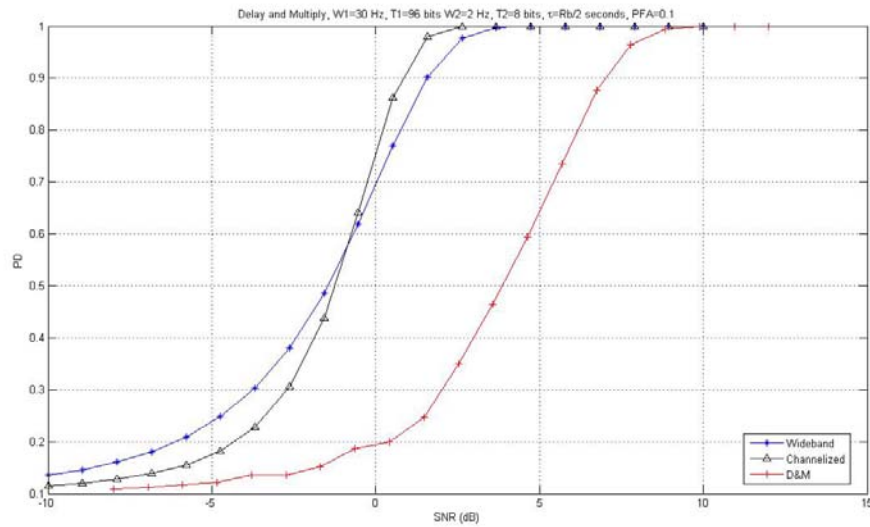


Figure A.1 Baseline D&M

The above Figure used the same  $T_1=96$  bits and  $W_2=30$  Hz parameters as the Chapter 4 simulations. The D&M receiver was approximately 5.9 dB worse than the wideband radiometer at  $P_D=0.9$ .

## A.2 Reducing Signal Duration

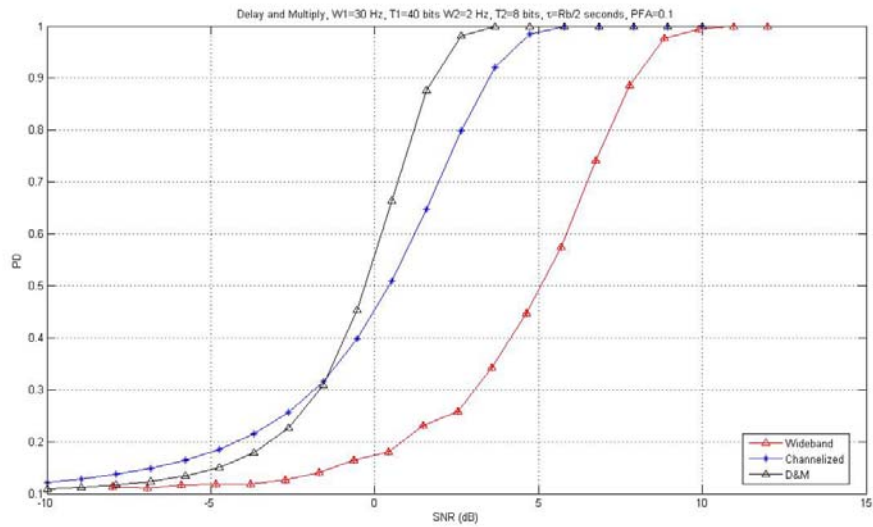


Figure A.2 D&M Reduction in  $T_1$  from 96 to 40 Bits

As Figure A.2 shows, reducing the signal duration to  $T_1=40$  bits improved the D&M receiver's relative performance by 1.5 dB, but it was still 4.4 dB poorer than the wideband radiometer.

### A.3 Reducing Hop Rate

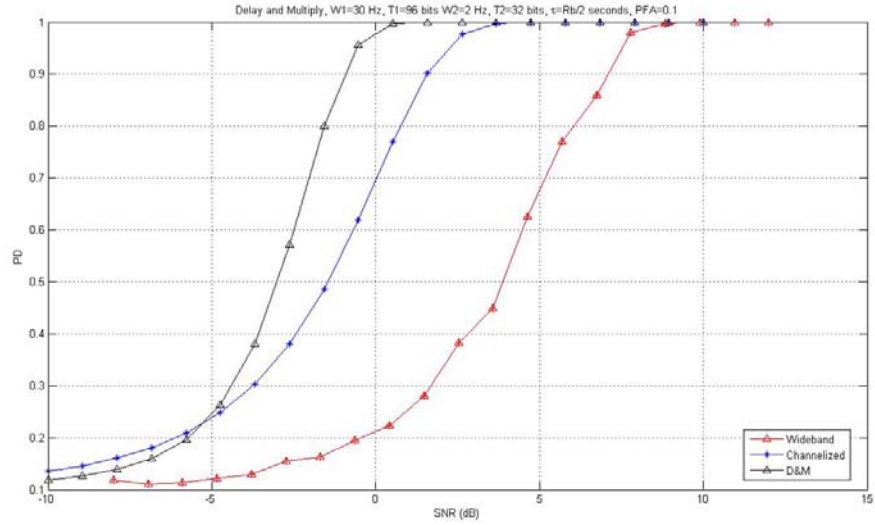


Figure A.3 D&M Reduction in Hop Rate from 1/8 to 1/32 Seconds

Figure A.3 shows the D&M receiver was not significantly affected by the change in hop rate, much like the wideband radiometer. It remained 5.9 dB poorer than the wideband radiometer.

### A.4 Introducing Wideband Jamming

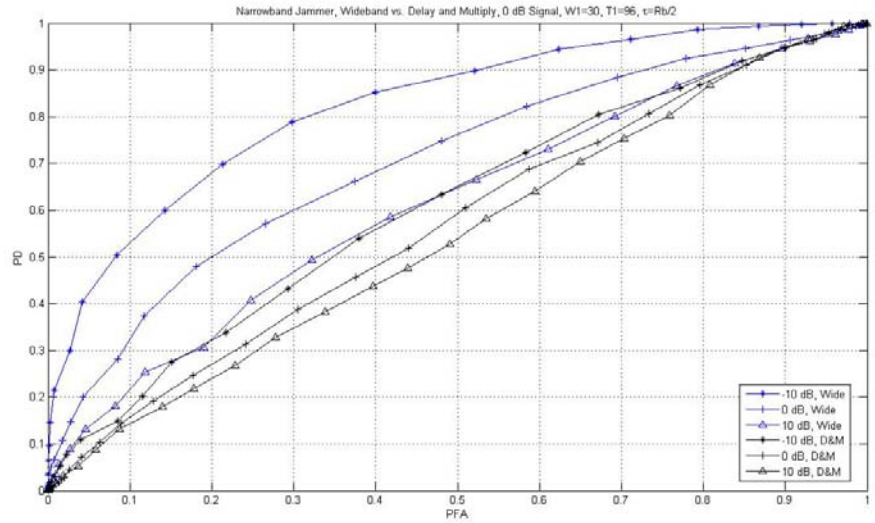


Figure A.4 D&M With Wideband Jamming

When placed in a wideband jamming environment, the D&M receiver does not perform very well. While the channelized radiometer improved relative to the wideband radiometer under the influence of wideband jamming, the D&M receiver registers a near  $P_{FA}=P_D$  line in the ROC curve.

Thus, with the results shown in this Appendix, it is clear that the D&M receiver should not be considered a candidate receiver design when used in conjunction with GMSK-FH signals with structures similar to the signal of interest used in this research.

## Appendix B. MATLAB Code

```
%%%%%%%%%%%%%%%%%%%%%%%%%%%%%%%%%%%%%%%%%%%%%%%%%%%%%%%%%%%%%%%%%%%%%%%%
% Clint R. Sikes
% EENG 799
% Wideband Radiometer Theory
%%%%%%%%%%%%%%%%%%%%%%%%%%%%%%%%%%%%%%%%%%%%%%%%%%%%%%%%%%%%%%%%%%%%%%%%

clear;clc;

%%%%%%%%%%%%%%%%%%%%%%%%%%%%%%%%%%%%%%%%%%%%%%%%%%%%%%%%%%%%%%%%%%%%%%%%
%Simulation Parameters
%%%%%%%%%%%%%%%%%%%%%%%%%%%%%%%%%%%%%%%%%%%%%%%%%%%%%%%%%%%%%%%%%%%%%%%%

jitter=0; %'1' If Using Jitter, '0' If Not
snr_db=linspace(-10,10,20); %SNR in dB
snr=10.^(snr_db./10); %SNR
T=96; %T1
W=30; %W1
pct_jitter=0.25; %Percentage of Jitter
if jitter==1
    multifact=T2./(T2-pct_jitter.*T2);
    multifact=1./multifact;
else
    multifact=1;
end

PFA=0.01; %Desired CFAR PFA

%%%%%%%%%%%%%%%%%%%%%%%%%%%%%%%%%%%%%%%%%%%%%%%%%%%%%%%%%%%%%%%%%%%%%%%%
%Simulation
%%%%%%%%%%%%%%%%%%%%%%%%%%%%%%%%%%%%%%%%%%%%%%%%%%%%%%%%%%%%%%%%%%%%%%%%

for i=1:length(snr)
    PD(i)=qfunc(qfuncinv(PFA)-multifact*snr(i)/sqrt(W/T));
end

figure(1)
plot(snr_db,PD(1,:), 'r-*');
xlabel('SNR_req (dB)');
ylabel('PD');
title('Wideband Radiometer, T1=96, W1=30, PFA=0.01');
grid on
hold on
```

```

%%%%%%%%%%%%%%%%%%%%%%%%%%%%%%%%%%%%%%%%%%%%%%%%%%%%%%%%%%%%%%%%%%%%%%%%
% Clint R. Sikes
% EENG 799
% Channelized Radiometer Theory
%%%%%%%%%%%%%%%%%%%%%%%%%%%%%%%%%%%%%%%%%%%%%%%%%%%%%%%%%%%%%%%%%%%%%%%%

clear;clc;

%%%%%%%%%%%%%%%%%%%%%%%%%%%%%%%%%%%%%%%%%%%%%%%%%%%%%%%%%%%%%%%%%%%%%%%%
%Simulation Parameters
%%%%%%%%%%%%%%%%%%%%%%%%%%%%%%%%%%%%%%%%%%%%%%%%%%%%%%%%%%%%%%%%%%%%%%%%

jitter=1; %'1' If Using Jitter, '0' If Not
M=15; %Number of Channels
N=12; %Number of Hops
kN=ceil(0.6*N) %Hop Threshold
snr_db=linspace(-10,10,20); %snr per hop in dB
snr=10.^(snr_db./10); %snr per hop
T2=8; %T2
W2=0.3; %W2
pct_jitter=0.25; %Amount of Jitter
if jitter==1
    multifact=T2./(T2-pct_jitter.*T2);
    multifact=1./multifact;
else
    multifact=1;
end

PFA_desired=0.01 %Desired PFA

%%%%%%%%%%%%%%%%%%%%%%%%%%%%%%%%%%%%%%%%%%%%%%%%%%%%%%%%%%%%%%%%%%%%%%%%
%Simulation
%%%%%%%%%%%%%%%%%%%%%%%%%%%%%%%%%%%%%%%%%%%%%%%%%%%%%%%%%%%%%%%%%%%%%%%%

QF=linspace(0.002,.05,1000);
for i=1:length(snr_db)
    clear PF_1
    clear PD_1
    QD(i,:)=qfunc(qfuncinv(QF)-...
        sqrt(16*T2^2*(multifact*snr(i))^2/(16*T2*W2+8*T2*multifact*snr(i))));
    p0(i,:)=1-(1-QF).^M;
    p1(i,:)=1-(1-QD(i,:)).*(1-QF).^(M-1);
    for n=kN:N
        PF_1(n-kN+1,:)=factorial(N)./(factorial(N-
n).*factorial(n)).*p0(i,).^n.*(1-p0(i,)).^(N-n);
        PD_1(n-kN+1,:)=factorial(N)./(factorial(N-
n).*factorial(n)).*p1(i,).^n.*(1-p1(i,)).^(N-n);
    end
    PFA(i,:)=sum(PF_1);
    PD(i,:)=sum(PD_1);
end

for i=1:length(snr)
    [c,Zt]=min(abs(PFA(i,:)-PFA_desired));
    final_PFA(i)=PFA(i,Zt);
    final_QF(i)=QF(Zt);
    final_PD(i)=PD(i,Zt);
end

figure(1)
plot(snr_db,final_PD(1,:), 'k-*');
grid on

```

```

%%%%%%%%%%%%%%%%%%%%%%%%%%%%%%%%%%%%%%%%%%%%%%%%%%%%%%%%%%%%%%%%%%%%%%%%
% Clint R. Sikes
% EENG 799
% Wideband Radiometer Simulation
%%%%%%%%%%%%%%%%%%%%%%%%%%%%%%%%%%%%%%%%%%%%%%%%%%%%%%%%%%%%%%%%%%%%%%%%

clear;clc;

%%%%%%%%%%%%%%%%%%%%%%%%%%%%%%%%%%%%%%%%%%%%%%%%%%%%%%%%%%%%%%%%%%%%%%%%
%Simulation Parameters
%%%%%%%%%%%%%%%%%%%%%%%%%%%%%%%%%%%%%%%%%%%%%%%%%%%%%%%%%%%%%%%%%%%%%%%%

jitmode=0; %'1' If Using Jitter, '0' If Not
bitrate=2; %Bitrate in Mbps
pulselength=48; %Length of pulse in microseconds
L=3; %Length of GMSK Pulse Shape
Ts=2/bitrate; %Symbol Period, Default is 1 at 2Mbps
BT=0.3; %BT Parameter of GMSK Pulse
h=0.5; %Modulation Index of GMSK Pulse
z0=0; %Initial Phase of GMSK Signal
fcvec=[2 4 6 8 10 12 14 16 18 20 22 24 26 28 30]; %Possible Hop Freqs
fc=max(fcvec);
fs=fc*4; %Number of Samples/Second
ns=fs*Ts; %Number of samples/bit
pct_jitter=0.25; %Percent Jitter offset
hoprate=8; %T2
jitter=pct_jitter*hoprate*ns; %of samples to offset in one hop
N=pulselength*bitrate; %Number of bits in T1
ebno_db=linspace(-10,10,20);
nosamp=10; %Arbitrary Value to be Noise Power
ebno=10.^(ebno_db./10);
snr=2.*ebno./ns;
esym=nosamp^2.*snr.*Ts; %Signal Power as Scaled From Noise Power
numtrials=10000; %Number of Simulations to Perfrom
PFA_desired=0.01 %Desired CFAR PFA

tic
for k=1:length(ebno_db)
    clear sGMSK;
    clear bits;

    %Generating vector of binary bits
    bitsin=round(rand(1,N))';

    %Converting bits to NRZ
    for i=1:N
        if bitsin(i)==0
            bits(i)=-1;
        else
            bits(i)=1;
        end
    end

    bits=bits';

    %Generate GMSK Pulse Shape
    tpulse=[-1.5*Ts:1/fs:1.5*Ts-1/fs];
    g=1/(2*Ts).*(qfunc(2*pi*BT.*(tpulse-Ts/2)./(Ts*sqrt(log(2)))))-...
        qfunc(2*pi*BT.*(tpulse+Ts/2)./(Ts*sqrt(log(2)))));
    g=g/(2*sum(g));

    Zn=0;
    Zs=0;
end

```

```

%Generate SOI
for i=1:numtrials

[fcout, Phase, sGMSK]=gmskmod_slowhop(L, bits, ns, fcvec, Ts, hoprate, N, BT, g, h);
    if jitmode==1
        for v=1:N/hoprate
            jGMSK((v-1)*ns*hoprate+1:v*ns*hoprate)=[sGMSK((v-
1)*ns*hoprate+1:v*ns*hoprate-jitter) zeros(1,jitter)];
        end
    else
        jGMSK=sGMSK;
    end
    %Changing SNR by varying Signal Power
    new_sGMSK=esym(k).*jGMSK;
    new_noise = nosamp.*randn(size(new_sGMSK));
    new_noisy_GMSK=new_sGMSK+new_noise;

    %Signal Plus Noise Section
    %Truncating in Time (T1)
    trunc_GMSK=new_noisy_GMSK(1:end);
    [GMSKspec, f]=fft_ctr(trunc_GMSK, fs);
    centerbin=round(length(GMSKspec)/2);
    resolution=fs/length(GMSKspec);
    %Trauncating in Frequency (W1)

GMSKfilt=GMSKspec(centerbin+ceil(1/resolution):centerbin+ceil(31/resolution));
GMSK_square=abs(GMSKfilt).^2;

    %Noise Only Section
    %Truncating in Time (T1)
    trunc_noise=new_noise(1:end);
    [noisespec, f]=fft_ctr(trunc_noise, fs);
    %Trauncating in Frequency (W1)

noisefilt=noisespec(centerbin+ceil(1/resolution):centerbin+ceil(31/resolution)
);
    noise_square=abs(noisefilt).^2;

    %Test Statistics
    Zs(i)=sum(GMSK_square);
    Zn(i)=sum(noise_square);

end

%Thresholding
vecsort=sort(Zn);
Zt(k)=vecsort(numtrials-PFA_desired*numtrials);
n_ind=find(Zn>Zt(k));
PFA(k)=length(n_ind)/length(Zn);
s_ind=find(Zs>Zt(k));
PD(k)=length(s_ind)/length(Zs);

end

figure(1)
plot(ebno_db, PD, 'k-^')
xlabel('Eb/N0 (dB)');
ylabel('PD');
title('ROC Curves for Wideband Radiometer');
hold on
grid on

```



```

%%%%%%%%%%%%%%%%%%%%%%%%%%%%%%%%%%%%%%%%%%%%%%%%%%%%%%%%%%%%%%%%%%%%%%%%
% Clint R. Sikes
% EENG 799
% Channelized Radiometer Simulation
%%%%%%%%%%%%%%%%%%%%%%%%%%%%%%%%%%%%%%%%%%%%%%%%%%%%%%%%%%%%%%%%%%%%%%%%

clear;clc;

%%%%%%%%%%%%%%%%%%%%%%%%%%%%%%%%%%%%%%%%%%%%%%%%%%%%%%%%%%%%%%%%%%%%%%%%
%Simulation Parameters
%%%%%%%%%%%%%%%%%%%%%%%%%%%%%%%%%%%%%%%%%%%%%%%%%%%%%%%%%%%%%%%%%%%%%%%%

jitmode=0; %'1' If Using Jitter, '0' If Not
bitrate=2; %Bitrate in Mbps
pulselength=48; %Length of pulse in microseconds
L=3; %Length of GMSK Pulse Shape
Ts=2/bitrate; %Symbol Period, Default is 1 at 2Mbps
BT=0.3; %BT Parameter of GMSK Pulse
h=0.5; %Modulation Index of GMSK Pulse
z0=0; %Initial Phase of GMSK Signal
fcvec=[2 4 6 8 10 12 14 16 18 20 22 24 26 28 30]; %Possible Hop Freqs
fc=max(fcvec);
fs=fc*4; %Number of Samples/Second
ns=fs*Ts; %Number of samples/bit
pct_jitter=0.25; %Percent Jitter offset
hoprate=8; %T2
jitter=pct_jitter*hoprate*ns3; %#of samples to offset in one hop
N=pulselength*bitrate; %Number of bits in T1
ebno_db=linspace(-10,10,20);
nosamp=10; %Arbitrary Value to be Noise Power
Zt=2.376e6; %First Threshold, Determined Analytically
kN=.6*floor(N/hoprate);
ebno=10.^(ebno_db./10);
snr=2.*ebno./ns;
esym=nosamp^2.*snr.*Ts; %Signal Power as Scaled From Noise Power
numtrials=10000; %Number of Simulations to Perfrom

tic

for k=1:length(ebno_db)
clear sGMSK;
clear bits;

%Generating vector of binary bits
bitsin=round(rand(1,N))';

%Converting bits to NRZ
for i=1:N
if bitsin(i)==0
bits(i)=-1;
else
bits(i)=1;
end
end

bits=bits';

%Generate GMSK Pulse Shape
tpulse=[-1.5*Ts:1/fs:1.5*Ts-1/fs];
g=1/(2*Ts).* (qfunc(2*pi*BT.*(tpulse-Ts/2)./(Ts*sqrt(log(2)))))-...
qfunc(2*pi*BT.*(tpulse+Ts/2)./(Ts*sqrt(log(2)))));
g=g/(2*sum(g));

```

```

Znf=0;
Zsf=0;

%Generate SOI
for i=1:numtrials

[fcout, Phase, sGMSK]=gmskmod_slowhop(L, bits, ns, fcvec, Ts, hoprate, N, BT, g, h);
    if jitmode==1
        for v=1:N/hoprate
            jGMSK((v-1)*ns*hoprate+1:v*ns*hoprate)=[sGMSK((v-
1)*ns*hoprate+1:v*ns*hoprate-jitter) zeros(1,jitter)];
        end
    else
        jGMSK=sGMSK;
    end

    %Changing SNR by varying Signal Power
    new_sGMSK=sqrt(2.*esym(k)).*jGMSK;
    new_noise = nosamp.*randn(size(new_sGMSK));
    new_noisy_GMSK=new_sGMSK+new_noise;
    centerbin=length(new_noisy_GMSK)/2;

    %Creating a Space Full of Statistics
    for r=1:floor(N/hoprate)

        for j=1:length(fcvec)

            %Signal Plus Noise Section
            %Truncating in Time (T2)
            GMSK_trunc=new_noisy_GMSK((r-1)*ns*hoprate+1:r*ns*hoprate);
            [GMSKspec, f3]=fft_ctr(GMSK_trunc, fs);
            centerbin=round(length(GMSKspec)/2);
            resolution=fs/length(GMSKspec);
            %Truncating in Frequency (W2)
            GMSKfilt=GMSKspec(centerbin+ceil((j*2-
1)/resolution):centerbin+ceil((j*2+1)/resolution));
            Zs(j, r)=sum(abs(GMSKfilt).^2);

            %Noise-Only Section
            %Truncating in Time (Exactly One Hop)
            noise_trunc=new_noise((r-1)*ns*hoprate+1:r*ns*hoprate);
            [noisespec, f3]=fft_ctr(noise_trunc, fs);
            %Truncating in Frequency (Exactly One Channel)
            noisefilt=noisespec(centerbin+ceil((j*2-
1)/resolution):centerbin+ceil((j*2+1)/resolution));
            %noisefilt=ifft(noisespec(centerbin:end));
            Zn(j, r)=sum(abs(noisefilt).^2);
        end
    end

    for r=1:floor(N/hoprate)
        for j=1:length(fcvec)

            %Summing over each hop (*Block is T2xW2)
            %Using a fixed per-cell FAR based on wideband claculations
            %Initial Test Statistics
            if Zs(j, r)>Zt
                sigblock(j, r)=1;
            else sigblock(j, r)=0;
            end
        end
    end
end

```

```

        if Zn(j,r)>Zt
            noiseblock(j,r)=1;
        else
            noiseblock(j,r)=0;
        end
    end
end

%Summing Along W (*detection is T2xW1)
%*Using Binary OR*
if sum(sigblock(:,r))>=1
    sigdetection(r)=1;
else
    sigdetection(r)=0;
end
if sum(noiseblock(:,r))>=1
    noisedetection(r)=1;
else
    noisedetection(r)=0;
end
end

%Summing Along T (*accum is T1*W1)
%Generates Final Test Statistics
Zsf(i)=sum(sigdetection);
Znf(i)=sum(noisedetection);
end

%Final Thresholding
n_ind=find(Znf>kN);
PFA(k)=length(n_ind)/length(Znf);
s_ind=find(Zsf>kN);
PD(k)=length(s_ind)/length(Zsf);
end

figure(1)
plot(ebno_db,PD,'-o')
xlabel('Ebno');
ylabel('PD');
title('ROC Curves for Channelized Radiometer, Binary-OR');
hold on
grid on

toc

```

```

%%%%%%%%%%%%%%%%%%%%%%%%%%%%%%%%%%%%%%%%%%%%%%%%%%%%%%%%%%%%%%%%%%%%%%%%
% Clint R. Sikes
% EENG 799
% Wideband Radiometer Simulation With Wideband Jamming
%%%%%%%%%%%%%%%%%%%%%%%%%%%%%%%%%%%%%%%%%%%%%%%%%%%%%%%%%%%%%%%%%%%%%%%%

clear;clc;

%%%%%%%%%%%%%%%%%%%%%%%%%%%%%%%%%%%%%%%%%%%%%%%%%%%%%%%%%%%%%%%%%%%%%%%%
%Simulation Parameters
%%%%%%%%%%%%%%%%%%%%%%%%%%%%%%%%%%%%%%%%%%%%%%%%%%%%%%%%%%%%%%%%%%%%%%%%

bitrate=2; %Bitrate in Mbps
pulselength=48; %Length of pulse in microseconds
L=3; %Length of GMSK Pulse Shape
Ts=2/bitrate; %Symbol Period, Default is 1 at 2Mbps
BT=0.3; %BT Parameter of GMSK Pulse
h=0.5; %Modulation Index of GMSK Pulse
z0=0; %Initial Phase of GMSK Signal
fcvec=[2 4 6 8 10 12 14 16 18 20 22 24 26 28 30]; %Possible Hop Freqs
fc=max(fcvec);
fs=fc*4; %Number of Samples/Second
ns=fs*Ts; %Number of samples/bit
hoprate=8; %T2
N=pulselength*bitrate; %Number of bits in T1
ebno_db=linspace(-10,10,20);
nosamp=10; %Arbitrary Value to be Noise Power
ebno=0;
snr=2.*ebno./ns;
esym=nosamp^2.*snr.*Ts; %Signal Power as Scaled From Noise Power
numtrials=10000; %Number of Simulations to Perfrom
noisevar=[0 0.25 0.5]; %Amount of change in noise floor during each trial
ROC_step=30; %Number of Data Points in ROC Curve

for k=1:length(noisevar)
    clear sGMSK;
    clear bits;

    %Generating vector of binary bits
    bitsin=round(rand(1,N))';

    %Converting bits to NRZ
    for i=1:N
        if bitsin(i)==0
            bits(i)=-1;
        else
            bits(i)=1;
        end
    end

    bits=bits';

    %Generate GMSK Pulse Shape
    tpulse=[-1.5*Ts:1/fs:1.5*Ts-1/fs];
    g=1/(2*Ts).*(qfunc(2*pi*BT.*(tpulse-Ts/2)./(Ts*sqrt(log(2)))))-...
        qfunc(2*pi*BT.*(tpulse+Ts/2)./(Ts*sqrt(log(2)))));
    g=g/(2*sum(g));

    tic

    Zn=0;
    Zs=0;
    for i=1:numtrials
        if randn(1)>0

```

```

        noiselevel(i)=sqrt(nosamp^2+(noisevar(k)*rand(1)*nosamp^2));
    else
        noiselevel(i)=sqrt(nosamp^2-(noisevar(k)*rand(1)*nosamp^2));
    end

    %Generate SOI

[fcout, Phase, sGMSK]=gmskmod_slowhop(L, bits, ns, fcvec, Ts, hoprate, N, BT, g, h);
new_GMSK=sqrt(2*esym).*sGMSK;
new_noise = noiselevel(i)*randn(size(new_GMSK));
new_noisy_GMSK=new_GMSK+new_noise;

%Signal Plus Noise Case
%Truncating in Time (T1)
trunc_GMSK=new_noisy_GMSK(1:end);
[GMSKspec, f]=fft_ctr(trunc_GMSK, fs);
centerbin=round(length(GMSKspec)/2);
resolution=fs/length(GMSKspec);
%Truncating in Frequency (W1)

GMSKfilt=GMSKspec(centerbin+ceil(1/resolution):centerbin+ceil(31/resolution));
GMSK_square=abs(GMSKfilt).^2;

%Noise Only Case
%Truncating in Time (T1)
trunc_noise=new_noise(1:end);
[noisespec, f]=fft_ctr(trunc_noise, fs);
%Truncating in Frequency (W1)

noisefilt=noisespec(centerbin+ceil(1/resolution):centerbin+ceil(31/resolution)
);
noise_square=abs(noisefilt).^2;

%Generate Test Statistics
Zs(i)=sum(GMSK_square);
Zn(i)=sum(noise_square);
end

stepsize=(max(Zs)-min(Zn))/ROC_step;
Zt(k, :)= [min(Zn):stepsize:max(Zs)];

%Thresholding
for i=1:ROC_step
    n_ind=find(Zn>Zt(k, i));
    PFA(k, i)=length(n_ind)/length(Zn);
    s_ind=find(Zs>Zt(k, i));
    PD(k, i)=length(s_ind)/length(Zs);
end

end

figure(1)
plot(PFA(1, :), PD(1, :), '-o')
xlabel('PFA');
ylabel('PD');
title('ROC Curves for Wideband Radiometer, \tau=1 hop (8 Symbols), W=1 freq
bin');
hold on
plot(PFA(2, :), PD(2, :), 'r-o')
hold on
plot(PFA(3, :), PD(3, :), 'k-o')
legend('none', '25%', '50%', 'location', 'se');

```

```

%%%%%%%%%%%%%%%%%%%%%%%%%%%%%%%%%%%%%%%%%%%%%%%%%%%%%%%%%%%%%%%%%%%%%%%%
% Clint R. Sikes
% EENG 799
% Channelized Radiometer Simulation With Wideband Jamming
%%%%%%%%%%%%%%%%%%%%%%%%%%%%%%%%%%%%%%%%%%%%%%%%%%%%%%%%%%%%%%%%%%%%%%%%

clear;clc;

%%%%%%%%%%%%%%%%%%%%%%%%%%%%%%%%%%%%%%%%%%%%%%%%%%%%%%%%%%%%%%%%%%%%%%%%
%Simulation Parameters
%%%%%%%%%%%%%%%%%%%%%%%%%%%%%%%%%%%%%%%%%%%%%%%%%%%%%%%%%%%%%%%%%%%%%%%%

bitrate=2; %Bitrate in Mbps
pulselength=48; %Length of pulse in microseconds
L=3; %Length of GMSK Pulse Shape
Ts=2/bitrate; %Symbol Period, Default is 1 at 2Mbps
BT=0.3; %BT Parameter of GMSK Pulse
h=0.5; %Modulation Index of GMSK Pulse
z0=0; %Initial Phase of GMSK Signal
fcvec=[2 4 6 8 10 12 14 16 18 20 22 24 26 28 30]; %Possible Hop Freqs
fc=max(fcvec);
fs=fc*4; %Number of Samples/Second
ns=fs*Ts; %Number of samples/bit
hoprate=8; %T2
N=pulselength*bitrate; %Number of bits in T1
kN=.6*floor(N/hoprate);
ebno_db=0;
nosamp=10; %Arbitrary Value to be Noise Power
ebno=10.^(ebno_db./10);
snr=2.*ebno./ns;
esym=nosamp^2.*snr.*Ts; %Signal Power as Scaled From Noise Power
numtrials=10000; %Number of Simulations to Perfrom
noisevar=[0 0.25 0.5]; %% change in noise floor during each trial
Zt=[linspace(1.8e6,2.8e6,30);linspace(1.6e6,3e6,30);linspace(1.3e6,3.2e6,30)];
ROC_step=30; %Number of Data Points in ROC Curve

tic

for k=1:length(noisevar)
clear sGMSK;
clear bits;

%Generating vector of binary bits
bitsin=round(rand(1,N))';

%Converting bits to NRZ
for i=1:N
if bitsin(i)==0
bits(i)=-1;
else
bits(i)=1;
end
end

bits=bits';

%Generate GMSK Pulse Shape
tpulse=[-1.5*Ts:1/fs:1.5*Ts-1/fs];
g=1/(2*Ts).*(qfunc(2*pi*BT.*(tpulse-Ts/2)./(Ts*sqrt(log(2)))))-...
qfunc(2*pi*BT.*(tpulse+Ts/2)./(Ts*sqrt(log(2)))));
g=g/(2*sum(g));

```

```

Zn=0;
Zs=0;
for i=1:numtrials %Varying noise floor. SigPower remains the same
    if randn(1)>0
        noiselevel(i)=sqrt(nosamp^2+(noisevar(k)*rand(1)*nosamp^2));
    else
        noiselevel(i)=sqrt(nosamp^2-(noisevar(k)*rand(1)*nosamp^2));
    end
    %Generate SOI

[fcout,Phase,sGMSK]=gmskmod_slowhop(L,bits,ns,fcvec,Ts,hoprate,N,BT,g,h);
%Changing SNR by varying esym
new_sGMSK=sqrt(2.*esym).*sGMSK;
new_noise = noiselevel(i).*randn(size(new_sGMSK));
new_noisy_GMSK=new_sGMSK+new_noise;

centerbin=length(new_noisy_GMSK)/2;

%Creating a Space Full of Statistics
for r=1:floor(N/hoprate)

    for j=1:length(fcvec)

        %Signal Plus Noise Case
        %Truncating in Time (Exactly One Hop)
        GMSK_trunc=new_noisy_GMSK((r-1)*ns*hoprate+1:r*ns*hoprate);
        [GMSKspec,f]=fft_ctr(GMSK_trunc,fs);
        centerbin=round(length(GMSKspec)/2);
        resolution=fs/length(GMSKspec);
        %Truncating in Frequency (Exactly One Channel)
        GMSKfilt=GMSKspec(centerbin+ceil((j*2-
1)/resolution):centerbin+ceil((j*2+1)/resolution));
        Zs(j,r)=sum(abs(GMSKfilt).^2);

        %Noise Only Case
        %Truncating in Time (Exactly One Hop)
        noise_trunc=new_noise((r-1)*ns*hoprate+1:r*ns*hoprate);
        [noisespec,f]=fft_ctr(noise_trunc,fs);
        %Truncating in Frequency (Exactly One Channel)
        noisefilt=noisespec(centerbin+ceil((j*2-
1)/resolution):centerbin+ceil((j*2+1)/resolution));
        Zn(j,r)=sum(abs(noisefilt).^2);
    end
end

for w=1:ROC_step
    for r=1:floor(N/hoprate)
        for j=1:length(fcvec)

            %Summing over each hop (*Block is T2xW2)
            %Using a fixed per-cell FAR based on wideband claculations

            if Zs(j,r)>Zt(k,w)
                sigblock(j,r)=1;
            else sigblock(j,r)=0;
            end
            if Zn(j,r)>Zt(k,w)
                noiseblock(j,r)=1;
            else
                noiseblock(j,r)=0;
            end
        end

        %Summing Along W (*detection is T2xW1)

```

```

        %*Using Binary OR*
        if sum(sigblock(:,r))>=1
            sigdetection(r)=1;
        else
            sigdetection(r)=0;
        end
        if sum(noiseblock(:,r))>=1
            noisedetection(r)=1;
        else
            noisedetection(r)=0;
        end
    end

    %Summing Along T (*accum is T1*W1)
    %Generating Final Test Statistics
    Zsf(w,i)=sum(sigdetection);
    Znf(w,i)=sum(noisedetection);

end

end

%Thresholding
for w=1:ROC_step
    n_ind=find(Znf(w,:)>kN);
    PFA(k,w)=length(n_ind)/length(Zn);
    s_ind=find(Zsf(w,:)>kN);
    PD(k,w)=length(s_ind)/length(Zs);

end

end

figure(1)
plot(PFA(1,:),PD(1,:),'-o')
xlabel('PFA');
ylabel('PD');
title('ROC Curves for Channelized Radiometer (Threshlvar), Binary-OR');
hold on
plot(PFA(2,:),PD(2,:),'r-o')
hold on
plot(PFA(3,:),PD(3,:),'k-o')
legend('No change','25% Offset','50% Offset','location','se');
grid on

toc

```



```

%%%%%%%%%%%%%%%%%%%%%%%%%%%%%%%%%%%%%%%%%%%%%%%%%%%%%%%%%%%%%%%%%%%%%%%%
% Clint R. Sikes
% EENG 799
% Slow Sweeping Channelized Radiometer Simulation
%%%%%%%%%%%%%%%%%%%%%%%%%%%%%%%%%%%%%%%%%%%%%%%%%%%%%%%%%%%%%%%%%%%%%%%%

clear;clc;

%%%%%%%%%%%%%%%%%%%%%%%%%%%%%%%%%%%%%%%%%%%%%%%%%%%%%%%%%%%%%%%%%%%%%%%%
%Simulation Parameters
%%%%%%%%%%%%%%%%%%%%%%%%%%%%%%%%%%%%%%%%%%%%%%%%%%%%%%%%%%%%%%%%%%%%%%%%

bitrate=2; %Bitrate in Mbps
pulselength=48; %Length of pulse in microseconds
L=3; %Length of GMSK Pulse Shape
Ts=2/bitrate; %Symbol Period, Default is 1 at 2Mbps
BT=0.3; %BT Parameter of GMSK Pulse
h=0.5; %Modulation Index of GMSK Pulse
z0=0; %Initial Phase of GMSK Signal
fcvec=[2 4 6 8 10 12 14 16 18 20 22 24 26 28 30]; %Possible Hop Freqs
fc=max(fcvec);
fs=fc*4; %Number of Samples/Second
ns=fs*Ts; %Number of samples/bit
hoprate=8; %T2
N=pulselength*bitrate; %Number of bits in T1
ebno_db=linspace(-10,10,20);
nosamp=10; %Arbitrary Value to be Noise Power
Zt=2.376e6; %First Threshold, Determined Analytically
kN=.6*floor(N/hoprate);
ebno=10.^(ebno_db./10);
snr=2.*ebno./ns;
esym=nosamp^2.*snr.*Ts; %Signal Power as Scaled From Noise Power
numtrials=10000; %Number of Simulations to Perfrom
K=3; %Number of Hops for Complete Frequency Coverage

tic

for k=1:length(ebno_db)
    clear sGMSK;
    clear bits;

    %Generating vector of binary bits
    bitsin=round(rand(1,N))';

    %Converting bits to NRZ
    for i=1:N
        if bitsin(i)==0
            bits(i)=-1;
        else
            bits(i)=1;
        end
    end

    bits=bits';

    %Generate GMSK Pulse Shape
    tpulse=[-1.5*Ts:1/fs:1.5*Ts-1/fs];
    g=1/(2*Ts).*(qfunc(2*pi*BT.*(tpulse-Ts/2)./(Ts*sqrt(log(2)))))-...
        qfunc(2*pi*BT.*(tpulse+Ts/2)./(Ts*sqrt(log(2)))));
    g=g/(2*sum(g));

    Znf=0;

```

```

Zns=0;
for i=1:numtrials

    %Generate SOI

[fcout, Phase, sGMSK]=gmskmod_slowhop(L, bits, ns, fcvec, Ts, hoprate, N, BT, g, h);
    %Changing SNR by varying esym
    new_sGMSK=sqrt(2.*esym(k)).*sGMSK;
    new_noise = nosamp.*randn(size(new_sGMSK));
    new_noisy_GMSK=new_sGMSK+new_noise;

    centerbin=length(new_noisy_GMSK)/2;
    divisor=0; %Initializing frequency selector

    %Creating a Space Full of Statistics
    for r=1:floor(N/hoprate)
        p=mod(divisor,K)+1; %Sets p=1-->K to match fast sweeper case

        for j=1:length(fcvec)/K

            %Signal Plus Noise Case
            %Truncating in Time (Exactly One Hop)
            GMSK_trunc=new_noisy_GMSK((r-1)*ns*hoprate+1:r*ns*hoprate);
            [GMSKspec, f]=fft_ctr(GMSK_trunc, fs);
            centerbin=round(length(GMSKspec)/2);
            resolution=fs/length(GMSKspec);
            %Truncating in Frequency (Exactly One Channel)
            GMSKfilt=GMSKspec(centerbin+ceil((j*p*2-
1)/resolution):centerbin+ceil((j*p*2+1)/resolution));
            Zs(j, r)=sum(abs(GMSKfilt).^2);

            %Noise Only Case
            %Truncating in Time (Exactly One Hop)
            noise_trunc=new_noise((r-1)*ns*hoprate+1:r*ns*hoprate);
            [noisespec, f]=fft_ctr(noise_trunc, fs);
            %Truncating in Frequency (Exactly One Channel)
            noisefilt=noisespec(centerbin+ceil((j*p*2-
1)/resolution):centerbin+ceil((j*p*2+1)/resolution));
            Zn(j, r)=sum(abs(noisefilt).^2);
        end
        divisor=divisor+1;
    end

    for r=1:floor(N/hoprate)

        %Summing over each hop (*Block is T2xW2)
        %Using a fixed per-cell FAR based on wideband claculations
        %Intermediate Thresholding
        if max(Zs(:, r))>Zt
            sigdetection(r)=1;
        else sigdetection(r)=0;
        end
        if max(Zn(:, r))>Zt
            noisedetection(r)=1;
        else
            noisedetection(r)=0;
        end
    end

end

```

```

        %Summing Along T (*accum is T1*W1)
        %Generating Final Statistics
        Zns(i)=sum(sigdetection);
        Znf(i)=sum(noisedetection);

    end

    %Final Thresholding
    n_ind=find(Znf>kN);
    PFA(k)=length(n_ind)/length(Znf);
    s_ind=find(Zns>kN);
    PD(k)=length(s_ind)/length(Zns);

end

figure(1)
plot(ebno_db,PD,'-o')
xlabel('e $\bar{b}n_0$ ');
ylabel('PD');
title('ROC Curves for Channelized Radiometer, Maxbased');

toc

```

```

%%%%%%%%%%%%%%%%%%%%%%%%%%%%%%%%%%%%%%%%%%%%%%%%%%%%%%%%%%%%%%%%%%%%%%%%
% Clint R. Sikes
% EENG 799
% Fast Sweeping Channelized Radiometer Simulation
%%%%%%%%%%%%%%%%%%%%%%%%%%%%%%%%%%%%%%%%%%%%%%%%%%%%%%%%%%%%%%%%%%%%%%%%

clear;clc;

%%%%%%%%%%%%%%%%%%%%%%%%%%%%%%%%%%%%%%%%%%%%%%%%%%%%%%%%%%%%%%%%%%%%%%%%
%Simulation Parameters
%%%%%%%%%%%%%%%%%%%%%%%%%%%%%%%%%%%%%%%%%%%%%%%%%%%%%%%%%%%%%%%%%%%%%%%%

bitrate=2; %Bitrate in Mbps
pulselength=48; %Length of pulse in microseconds
L=3; %Length of GMSK Pulse Shape
Ts=2/bitrate; %Symbol Period, Default is 1 at 2Mbps
BT=0.3; %BT Parameter of GMSK Pulse
h=0.5; %Modulation Index of GMSK Pulse
z0=0; %Initial Phase of GMSK Signal
fcvec=[2 4 6 8 10 12 14 16 18 20 22 24 26 28 30]; %Possible Hop Freqs
fc=max(fcvec);
fs=fc*4; %Number of Samples/Second
ns=fs*Ts; %Number of samples/bit
hoprate=8; %T2
N=pulselength*bitrate; %Number of bits in T1
ebno_db=linspace(-10,10,20);
nosamp=10; %Arbitrary Value to be Noise Power
Zt=2.376e6; %First Threshold, Determined Analytically
kN=.6*floor(N/hoprate);
ebno=10.^(ebno_db./10);
snr=2.*ebno./ns;
esym=nosamp^2.*snr.*Ts; %Signal Power as Scaled From Noise Power
numtrials=10000; %Number of Simulations to Perfrom
K=3; %Number of Radiometer Hops per T2

tic

for k=1:length(ebno_db)
clear sGMSK;
clear bits;

numtrials=10000;

%Generating vector of binary bits
bitsin=round(rand(1,N))';

%Converting bits to NRZ
for i=1:N
if bitsin(i)==0
bits(i)=-1;
else
bits(i)=1;
end
end

bits=bits';

%Generate g
tpulse=[-1.5*Ts:1/fs:1.5*Ts-1/fs];
g=1/(2*Ts).*(qfunc(2*pi*BT.*(tpulse-Ts/2)./(Ts*sqrt(log(2)))))-...
qfunc(2*pi*BT.*(tpulse+Ts/2)./(Ts*sqrt(log(2)))));
g=g/(2*sum(g));

```

```

Znf=0;
Zsf=0;
for i=1:numtrials
    %Generate SOI

[fcout,Phase,sGMSK]=gmskmod_slowhop(L, bits, ns, fcvec, Ts, hoprate, N, BT, g, h);
    %Changing SNR by varying esym
    new_sGMSK=sqrt(2.*esym(k)).*sGMSK;
    new_noise = nosamp.*randn(size(new_sGMSK));
    new_noisy_GMSK=new_sGMSK+new_noise;

    centerbin=length(new_noisy_GMSK)/2;

    %Creating a Space Full of Statistics
    for r=1:floor(N/hoprate)

        for p=1:K

            for j=1:length(fcvec)/K

                %Signal Pus Noise Case
                %Truncating in Time (Exactly One Hop/K)
                GMSK_trunc=new_noisy_GMSK((r-1)*ns*hoprate+(p-
1)*ns*hoprate/K+1:r*ns*hoprate-(K-p)*ns*hoprate/K);
                [GMSKspec,f]=fft_ctr(GMSK_trunc,fs);
                centerbin=round(length(GMSKspec)/2);
                resolution=fs/length(GMSKspec);
                %Trauncating in Frequency (Exactly One Channel)
                GMSKfilt=GMSKspec(centerbin+ceil((j*p*2-
1)/resolution):centerbin+ceil((j*p*2+1)/resolution));
                Zs(j+(p-1)*length(fcvec)/K,r)=sum(abs(GMSKfilt).^2);

                %Noise Only Case
                %Truncating in Time (Exactly One Hop)
                noise_trunc=new_noise((r-1)*ns*hoprate+(p-
1)*ns*hoprate/K+1:r*ns*hoprate-(K-p)*ns*hoprate/K);
                [noisespec,f]=fft_ctr(noise_trunc,fs);
                %Truncating in Frequency (Exactly One Channel)
                noisefilt=noisespec(centerbin+ceil((j*p*2-
1)/resolution):centerbin+ceil((j*p*2+1)/resolution));
                Zn(j+(p-1)*length(fcvec)/K,r)=sum(abs(noisefilt).^2);
            end
        end
    end

    for r=1:floor(N/hoprate)

        %Summing over each hop (*Block is T2xW2)
        %Using a fixed per-cell FAR based on wideband claculations
        %Intermediate Thresholding
        if max(Zs(:,r))>Zt
            sigdetection(r)=1;
        else sigdetection(r)=0;
        end
        if max(Zn(:,r))>Zt
            noisedetection(r)=1;
        else
            noisedetection(r)=0;
        end
    end

    %Summing Along T (*accum is T1*W1)

```

```

    %Generate Final Test Statistics
    Zsf(i)=sum(sigdetection);
    Znf(i)=sum(noisedetection);

end

%Varying the Summing threshold
%Final Thresholding
n_ind=find(Znf>kN);
PFA(k)=length(n_ind)/length(Znf);
s_ind=find(Zsf>kN);
PD(k)=length(s_ind)/length(Zsf);

end

figure(1)
plot(ebno_db,PD,'-o')
xlabel('ebno');
ylabel('PD');
title('ROC Curves for Channelized Radiometer, Maxbased');

toc

```

```

%%%%%%%%%%%%%%%%%%%%%%%%%%%%%%%%%%%%%%%%%%%%%%%%%%%%%%%%%%%%%%%%%%%%%%%%
% Clint R. Sikes
% EENG 799
% Delay and Multiply Simulation
%%%%%%%%%%%%%%%%%%%%%%%%%%%%%%%%%%%%%%%%%%%%%%%%%%%%%%%%%%%%%%%%%%%%%%%%

clear;clc;

%%%%%%%%%%%%%%%%%%%%%%%%%%%%%%%%%%%%%%%%%%%%%%%%%%%%%%%%%%%%%%%%%%%%%%%%
%Simulation Parameters
%%%%%%%%%%%%%%%%%%%%%%%%%%%%%%%%%%%%%%%%%%%%%%%%%%%%%%%%%%%%%%%%%%%%%%%%

bitrate=2; %Bitrate in Mbps
pulselength=48; %Length of pulse in microseconds
L=3; %Length of GMSK Pulse Shape
Ts=2/bitrate; %Symbol Period, Default is 1 at 2Mbps
BT=0.3; %BT Parameter of GMSK Pulse
h=0.5; %Modulation Index of GMSK Pulse
z0=0; %Initial Phase of GMSK Signal
fcvec=[2 4 6 8 10 12 14 16 18 20 22 24 26 28 30]; %Possible Hop Freqs
fc=max(fcvec);
fs=fc*4; %Number of Samples/Second
ns=fs*Ts; %Number of samples/bit
hoprate=8; %T2
N=pulselength*bitrate; %Number of bits in T1
ebno_db=linspace(-10,10,20);
nosamp=10; %Arbitrary Value to be Noise Power
ebno=10.^(ebno_db./10);
snr=2.*ebno./ns;
esym=nosamp^2.*snr.*Ts; %Signal Power as Scaled From Noise Power
numtrials=1000; %Number of Simulations to Perfrom
PFA_desired=0.1

tic
for k=1:length(ebno_db)
    clear sGMSK;
    clear bits;

    %Generating vector of binary bits
    bitsin=round(rand(1,N))';

    %Converting bits to NRZ
    for i=1:N
        if bitsin(i)==0
            bits(i)=-1;
        else
            bits(i)=1;
        end
    end

    bits=bits';

    %Generate GMSK Pulse Shape
    tpulse=[-1.5*Ts:1/fs:1.5*Ts-1/fs];
    g=1/(2*Ts).*(qfunc(2*pi*BT.*(tpulse-Ts/2)./(Ts*sqrt(log(2)))))-...
        qfunc(2*pi*BT.*(tpulse+Ts/2)./(Ts*sqrt(log(2)))));
    g=g/(2*sum(g));

    Zn=0;
    Zs=0;
    for i=1:numtrials

        %Generate Signal

```

```

[fcout, Phase, sGMSK]=gmskmod_slowhop(L, bits, ns, fcvec, Ts, hoprate, N, BT, g, h);
new_sGMSK=sqrt(2*esym(k)).*sGMSK;
new_noise = nosamp.*randn(size(new_sGMSK));
new_noisy_GMSK=new_sGMSK+new_noise;

%Delay Signal
GMSK_delay=[new_noisy_GMSK(ns/2+1:end) new_noisy_GMSK(1:ns/2)];

%Signal Plus Noise Case
GMSK_delay=GMSK_delay.*new_noisy_GMSK;
[GMSKspec, f]=fft_ctr(GMSK_delay, fs);
centerbin=round(length(GMSKspec)/2);
resolution=fs/length(GMSKspec);
%Use Narrow Filter
GMSKfilt=GMSKspec(centerbin-
ceil(0.25/resolution):centerbin+ceil(0.25/resolution));

%Noise Only Case
noise_delay=[new_noise(ns/2+1:end) new_noise(1:ns/2)];
noise_delay=noise_delay.*new_noise;
[noisespec, f]=fft_ctr(noise_delay, fs);
%Use Narrow Filter
noisefilt=noisespec(centerbin-
ceil(0.25/resolution):centerbin+ceil(0.25/resolution));

%Generate Test Statistics
Zs(i)=sum(abs(GMSKfilt));
Zn(i)=sum(abs(noisefilt));

end

%Thresholding
vecsort=sort(Zn);
Zt(k)=vecsort(numtrials-PFA_desired*numtrials);
n_ind=find(Zn>Zt(k));
PFA(k)=length(n_ind)/length(Zn);
s_ind=find(Zs>Zt(k));
PD(k)=length(s_ind)/length(Zs);

end

figure(1)
plot(ebno_db, PD, 'r-^')
xlabel('Eb/N0 (dB)');
ylabel('PD');
title('ROC Curves for Chirate Dertector, \tau=ns3/2');
hold on
grid on

toc

```



```

function [fc,Qt,Rt] = gmskmod_dobson_hop(L,a,ns,fcvec,Ts,hoplength,N,BT,g,h);

%This Function Generates a GMSK FH Signal
%Adopted from a Script Created by Jocelyn Dobson

Rt=[];
fs=ns/Ts;
rd = zeros(L-1,1); % data vector tail
Q0 = 0; % phase at the end of the bit
% Generate the random data
datain = [rd; a];
rd = datain(N+1 : N+L-1);
% Generate the phase shape during one period T
% Phase segmentation, corresponding to q(t-iT) for i = 3 to 1
q = cumsum(g); % g is the Gaussian filter function
qq = reshape(q, ns, L)';
qq = qq(L:-1:1,:);
% First term of phase equation
Qt = pi*(datain(1:N)*qq(1,:) +datain(2:N+1)*qq(2,.)+datain(3:N+2)*qq(3,:));
Qt = reshape(Qt', 1, N*ns); % arrange into 1D vector
% Generate the phase offset at the end of bit
% Second term of phase equation
S = cumsum([Q0; datain(1:N)]);
Q0 = S(N+1); % save phase at end of last bit
S = S(1:N)'+pi/2; % normalise by pi/2
Q1 = S(ones(1, ns),:); % interpolation for sampling
Q1 = Q1(:)';
% Combine to give the final phase
Qt = (Qt + Q1).*(h/(1/2)); %Normalize by modulation Index "h"
%Create Hopping Vector
for j=1:ceil(N/hoplength)
    fc1 = ceil(rand(1)*length(fcvec));
    fc(j) = fcvec(fc1);
end

fc=kron(fc,ones(1,hoplength));

for i=1:N
    % Form signal to be transmitted
    n = [(i-1)*Ts:1/fs:i*Ts-1/fs]; % form time base
    I = cos(2*pi*fc(i)*n).*cos(Qt(fs*Ts*(i-1)+1:fs*Ts*i)); % in-phase
component
    Q = sin(2*pi*fc(i)*n).*sin(Qt(fs*Ts*(i-1)+1:fs*Ts*i)); % quadrature
component
    Rt_temp = I - Q; % transmitted signal
    Rt=[Rt Rt_temp];
end

```

```

function [jamout] = narrowjam(inbits,fc,nosamp,SNR,tsym,nsamp)
%
%This Function Creates a PSK Modulated Narrowjam Signal
%Adopted From a Script Made by Dr. Michael Temple
%and Modified by Ray Nelseon
%
wnot = 2*pi*fc; % Radian frequency of Carrier
snrat = 10^(SNR/10); % Calculate Ratio form of Input SNR
esym=nosamp^2.*snrat.*tsym;
sigamp = sqrt(2*esym/tsym); % Signal Component Amplitude

bitsin = inbits'; % Actual BITS INto the Modulator
%
% Calculate Number of Symbol Periods (nsym) in RDATA
%
bitsym = 1; % Number of bits/symbol = 1 for BPSK
rbits=length(bitsin);
nsym = rbits/bitsym;
tstep = tsym/nsamp;

% Create time vector
timvec = tstep*(0:nsamp-1);

% Create time matrix, T, from timvec
T = repmat(timvec',1,nsym);

% Create phase matrix, Phi, from bitsin
Phi = repmat((pi*bitsin),nsamp,1);

% Create Symbol matrix using T and Phi
Arg = wnot*T + Phi;
Symbol = sigamp*cos(Arg);

% Create SIGNAL VECTOR
jamout = reshape(Symbol,1,(nsym*nsamp));

```

```

function [X,f]=fft_ctr(x,fs)
% [X,f] = fft_ctr(x,fs)
%
%   this function computes FFT of signal vector, arranging
%   FFT and frequency vectors about 0 Hz
%
%   Inputs: x = input signal row vector
%           fs = sample frequency
%   Out:    X = FFT of x, shifted so that 0 Hz is in middle
%           f = frequency vector, symmetric about 0 Hz
%
%   Bob Mills, 23 Aug 94
%
N=length(x);    % get length of vectors
fk=fs/N;

fa=linspace(0,fs-fs/N,N);
fl=fa( : , 1:N/2 );
fr=fa( : , N/2+1:N )-fs;
f=[ fr' ; fl' ]';
X=fftshift( fft(x) );

```

## Bibliography

- [1] B. E. White, "Tactical Data Links, Air Traffic Management, and Software Programmable Radios", *Proceedings of the 18th Digital Avionics Systems Conference*, Vol. 1, pp. 5.C.5-1-5.C.5-8, November 1999.
- [2] B. Hicks, "Transforming Avionics Architecture to Support Network Centric Warfare", *Proceedings of the 23rd Digital Avionics Systems Conference*, Vol. 2, pp. 8.E.1-1-8.E.1.12, October 2004.
- [3] R.F. Mills, "Detectability Models and Waveform Design for Multiple-Access Low Probability of Intercept Networks", PhD Dissertation, University of Kansas, 1994.
- [4] Thierry Turletti, "GMSK in a Nutshell", Telemedia Networks and Systems Group LCS, MIT-TR, Apr 1996.
- [5] John G. Proakis, *Digital Communications*. Boston, MA: McGraw Hill, 2001.
- [6] R.F. Mills and G.E. Prescott, "A Comparison of Various Radiometer Detection Models", *IEEE Transactions on Aerospace and Electronic Systems*, Vol. 32, No. 1, pp. 467-473, January 1996.
- [7] R.A. Dillard and G.M. Dillard, *Detectability of Spread-Spectrum Signals*. Dedham MA: Artech House, 1989.
- [8] J. J. Lehtomäki, "Maximum Based Detection of Slow Frequency Hopping Signals", *IEEE Communication Letters*, Vol. 7, No. 5, pp. 201-203, May 2003.
- [9] T.W. Fields, D.L. Sharpin, and J.B. Tsui, "Digital Channelized IFM Receiver", *1994 IEEE National Telesystems Conference Proceedings*, pp. 87 - 90, 1994.
- [10] J. J. Lehtomäki, M. Juntti, and H. Saarnisaari, "Detection of Frequency Hopping Signals with a Sweeping Channelized Radiometer", *Conference Record of the Thirty-Eighth Asilomar Conference on Signals, Systems and Computers*, Volume 2, pp. 2178 - 2182, November 2004.
- [11] *LPI Vulnerability Susceptibility Testing Program*. Final Report. ITT Aerospace/Optical Division, Fort Wayne, IN, December 1986.
- [12] H. L. Van Trees, *Detection, Estimation, and Modulation Theory (Part 1)*. New York NY: John Wiley and Sons, 2001.
- [13] J. J. Lehtomäki, M. Juntti, and H. Saarnisaari, "CFAR Strategies for a Channelized Radiometer", *IEEE Signal Processing Letters*, Vol. 12, No. 1, pp. 13-16, January 2005.
- [14] Roger L. Peterson, *Introduction to Spread-Spectrum Communications*. Upper Saddle River NJ: Prentice Hall, 1995.
- [15] David L. Nicholson, *Spread Spectrum Signal Design*. Rockville MD: Computer Science Press, 1988.

**REPORT DOCUMENTATION PAGE**

*Form Approved  
OMB No. 074-0188*

The public reporting burden for this collection of information is estimated to average 1 hour per response, including the time for reviewing instructions, searching existing data sources, gathering and maintaining the data needed, and completing and reviewing the collection of information. Send comments regarding this burden estimate or any other aspect of the collection of information, including suggestions for reducing this burden to Department of Defense, Washington Headquarters Services, Directorate for Information Operations and Reports (0704-0188), 1215 Jefferson Davis Highway, Suite 1204, Arlington, VA 22202-4302. Respondents should be aware that notwithstanding any other provision of law, no person shall be subject to a penalty for failing to comply with a collection of information if it does not display a currently valid OMB control number.

**PLEASE DO NOT RETURN YOUR FORM TO THE ABOVE ADDRESS.**

<b>1. REPORT DATE (DD-MM-YYYY)</b> 23-03-2006		<b>2. REPORT TYPE</b> Master's Thesis		<b>3. DATES COVERED (From - To)</b> September 2004 - March 2006	
<b>4. TITLE AND SUBTITLE</b>  NON-COOPERATIVE DETECTION OF FREQUENCY-HOPPED GMSK SIGNALS				<b>5a. CONTRACT NUMBER</b>	
				<b>5b. GRANT NUMBER</b>	
				<b>5c. PROGRAM ELEMENT NUMBER</b>	
<b>6. AUTHOR(S)</b>  Sikes, Clint R., First Lieutenant, USAF				<b>5d. PROJECT NUMBER</b>	
				<b>5e. TASK NUMBER</b>	
				<b>5f. WORK UNIT NUMBER</b>	
<b>7. PERFORMING ORGANIZATION NAMES(S) AND ADDRESS(S)</b> Air Force Institute of Technology Graduate School of Engineering and Management (AFIT/EN) 2950 Hobson Way WPAFB OH 45433-7765				<b>8. PERFORMING ORGANIZATION REPORT NUMBER</b>  AFIT/GE/ENG/06-52	
<b>9. SPONSORING/MONITORING AGENCY NAME(S) AND ADDRESS(ES)</b> Mr. James P. Stephens AFRL/SNRW 2241 Avionics Circle, Bldg 620 WPAFB OH 45433-7321 (AFMC) (937) 255-5579 x3547				<b>10. SPONSOR/MONITOR'S ACRONYM(S)</b>	
				<b>11. SPONSOR/MONITOR'S REPORT NUMBER(S)</b>	
<b>12. DISTRIBUTION/AVAILABILITY STATEMENT</b> APPROVED FOR PUBLIC RELEASE; DISTRIBUTION UNLIMITED.					
<b>13. SUPPLEMENTARY NOTES</b>					
<b>14. ABSTRACT</b> Many current and emerging communication signals use Gaussian Minimum Shift Keyed (GMSK), Frequency-Hopped (FH) waveforms to reduce adjacent-channel interference while maintaining Low Probability of Intercept (LPI) characteristics. These waveforms appear in both military (Tactical Targeting Networking Technology, or TTNT) and civilian (Bluetooth) applications. This research develops wideband and channelized radiometer intercept receiver models to detect a GMSK-FH signal under a variety of conditions in a tactical communications environment. The signal of interest (SOI) and receivers have both fixed and variable parameters. Jamming is also introduced into the system to serve as an environmental parameter. These parameters are adjusted to examine the effects they have on the detectability of the SOI. The metric for detection performance is the distance the intercept receiver must be from the communication transmitter in order to meet a given set of intercept receiver performance criteria, e.g., $P_{FA}$ and $P_D$ . It is shown that the GMSK-FH waveform benefits from an increased hop rate, a reduced signal duration, and introducing jitter into the waveform. Narrowband jamming is also very detrimental to channelized receiver performance. The intercept receiver benefits from reducing the bandwidth of the channelized radiometer channels, although this requires precise <i>a priori</i> knowledge of the hop frequencies.					
<b>15. SUBJECT TERMS</b> Gaussian Minimum Shift Keying, Frequency Hopping, Low Probability of Intercept Communications, Signal Detection					
<b>16. SECURITY CLASSIFICATION OF:</b>			<b>17. LIMITATION OF ABSTRACT</b>  UU	<b>18. NUMBER OF PAGES</b>  108	<b>19a. NAME OF RESPONSIBLE PERSON</b> Robert F. Mills, AFIT/ENG
<b>REPORT</b> U	<b>ABSTRACT</b> U	<b>c. THIS PAGE</b> U			<b>19b. TELEPHONE NUMBER (Include area code)</b> (937) 255-6565, ext 4527; e-mail: Robert.Mills@afit.edu

**Standard Form 298 (Rev. 8-98)**  
Prescribed by ANSI Std. Z39-18